AVO inversion with a combination of series reversion and Gauss-Newton iteration

Jian Sun, Kristopher A.H. Innanen

ABSTACT

Fluid-property discrimination is always an important goal we desired in seismic exploration, and one of interested ways to achieve that is related to AVO/AVA analysis. Several non-linear AVO/AVA approximations were derived directly from Zoeppritz equation with the comparison discussed. Non-linear AVO inversion with a combination of series reversion and Gauss-Newton iteration is introduced at the end of the paper, and one of those approximations we derived is applied into non-linear AVO inversion on synthetic data using well-log. Ultimately, the comparison between non-linear inversion method and linear inversion was discussed.

INTRODUCTION

AVO/AVA analysis is a useful pre-stack tool and widely applied to estimate elastic subsurface parameters according to the amplitude varies versus offset or angle incidence. Poroelastic theory delineated by Biot (1941) and Gassmann (1951) present a great tool for understanding fluid-interacted rock, and there is a great literature summary published by Krief (1990). Russell (2003) described how to connect the fluid discrimination with AVO inversion, and starting with AVO approximations with bulk modulus, shear modulus and density proposed by Gray (1999), derived a new linear approximation in terms of fluid term, shear modulus and density variation. Zong (2012) presented a new linear AVO approximation using P- and S- wave moduli in Bayesian framework.

It's well known that the relationship of the elastic parameters and observed seismic data is a non-linear inverse problem. Commonly speaking, the least square method is a great way to solve the non-linear equation, and one of the least square methods is famous as the Gauss-Newton iterative method by calculating the gradient and the Hessian matrix. Furthermore, Innanen (2011) introduced the AVO approximation in velocity perturbation form and delineated the AVO formula in form of series expansion.

In this paper, starting with Zoeppritz (1919) equation, we derived a non-linear AVO approximation with P- and S- waves moduli both in perturbation form and in reflectivity (ratio) form. The accuracy comparison will be discussed and one of those approximations will be applied into the non-linear AVO algorithm. In addition to that, the AVO approximation formula is expanded as series reversion and delineated how each term in series related to AVO approximation. The Gauss-Newton iterative algorithm will be applied to achieve non-linear AVO inversion and the input initial value can be obtained by evaluating the first order equation in series reversion. At last, a synthetic data using well 12-27, collected by CREWES at Hussar, Alberta in September 2011, will be considered to examine the capability of the non-linear AVO inversion with a combination of series reversion and Gauss-Newton iteration based on the new AVO formula we derived in terms of P- and S- waves moduli.

BIOT-GASSMANN THEORY WITH P- AND S- MODULI

Many theories have been published concerning the relationship between compressional (P), shear (S) waves and the lithology, the petro-physical parameters. In isotropic, elastic non-porous media, a basic equation can connect P- and S- wave velocity with density and different kinds of modulus, which is well known and can be written as

$$V_p = \sqrt{\frac{\lambda+2\mu}{\rho}} = \sqrt{\frac{K+\frac{4}{3}\mu}{\rho}} = \sqrt{\frac{M}{\rho}} \tag{1}$$

$$V_s = \sqrt{\frac{\mu}{\rho}} \tag{2}$$

$$K = \lambda + \frac{2}{3}\mu \tag{3}$$

where ρ is the density, λ is the Lame coefficient, μ is the 2nd Lame coefficient or shear modulus defined as the ratio of the shear stress to shear strain, K is the bulk modulus, M is the P-wave modulus defined as the ratio of axial stress to axial strain in a uniaxial state (Mavko et al. 1993).

The poroelasticity theory of Biot (1941) and Gassmann (1951) are most frequently way to express the P- and S- wave velocity in terms of elastic moduli in porous saturated rocks. The Biot-Gassmann theory indicated that a porous rock in Figure 1 can be recognized by four major components: the rock matrix, the pore/fluid system, the dry-rock skeleton, and the saturated rock itself (Russell et al. 2003).

For a porous saturated rock, Biot (1941) and Gassmann (1951) derived the parameters relationship between saturated and dry rock, in terms of Lame parameter and bulk modulus, respectively. Those equations are knows as

$$\lambda_{sat} = \lambda_{dry} + \beta^2 M_V \tag{4}$$

$$K_{sat} = K_{dry} + \beta^2 M_V \tag{5}$$

where K_{sat} is the bulk modulus of the saturated rock, K_{dry} is the bulk modulus of the dry rock, β is the Biot coefficient, M_V is the modulus, or hydraulic pressure needed to force an amount of water into the formation without any change in formation volume.

As the fluid has no viscosity and equating equations (3), (4) and (5), in other words, it means that

$$\mu_{sat} = \mu_{dry} \tag{6}$$

where μ_{sat} and μ_{dry} are the shear moduli of saturated rock and dry rock, respectively.

Also, we can rewrite equations (4) and (5) in terms of P- and S- wave moduli,

$$M_{sat} = M_{dry} + \beta^2 M_V \tag{7}$$

where M_{sat} is the P-wave modulus of the saturated rock, and M_{dry} is the P-wave modulus of dry rock. The term $\beta^2 M_V$ represents the interaction of the fluid filling the

porosity with solid dry-rock in the formation (Krief et al. 1990). Same as Russell et al. (2003) delineated, we can rewrite the fluid term f in terms of M_{sat} and M_{dry},

$$f = \beta^2 M_V = M_{sat} - M_{dry} \tag{8}$$

Then, in porous saturated rock, following equations (1) and (2), P- and S- wave velocities can be calculated by

$$(V_p)_{sat} = \sqrt{\frac{M_{sat}}{\rho_{sat}}} = \sqrt{\frac{M_{dry}+f}{\rho_{sat}}} \tag{9}$$

$$(V_s)_{sat} = \sqrt{\frac{\mu_{sat}}{\rho_{sat}}} = \sqrt{\frac{\mu_{dry}}{\rho_{sat}}} \tag{10}$$

And the fluid term can be rewritten as

$$f = M_{sat} - \rho_{dry}\left(V_p\right)_{dry}^2 = M_{sat} - \gamma_{dry}^2 u_{dry} = M_{sat} - \gamma_{dry}^2 u_{sat} \tag{11}$$

where $\gamma_{dry}=(\frac{V_p}{V_s})_{dry}$ is the velocity ratio between P- and S- wave in dry-rock, which can be estimated and has been discussed by Russell (2003), $(V_p)_{sat}$ is the P-wave velocity in porous saturated rock, $(V_s)_{sat}$ is the S-wave velocity in porous saturated rock.

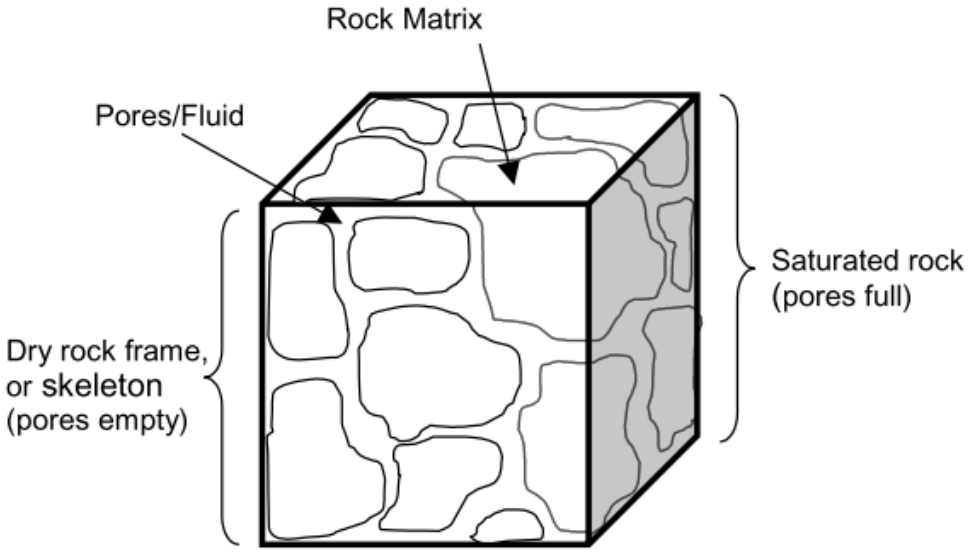

FIG.1. Four major components in a cube of rock with poroelasticity theory: the rock matrix, the pore/fluid system, the dry rock frame, and the saturated frame (Russell et al. 2003).

Consider those theories we reviewed above, the fluid term in porous saturated rock can be discriminated using P-, S- wave moduli and γ_{dry}. In next section, we will discuss how to connect AVO with P-, S- wave moduli start from Zoeppritz equation.

POROELASTICITY AVO/AVA APPROXIMATION IN MODULI

The response of an incidence P-wave between two elastic media (when angle incidence is greater than zero) can be delineated in Figure 2. And exact solutions for reflected (R_{pp} and R_{ps}) and transmitted (T_{pp} and T_{ps}) waves can be achieved by applying Zoeppritz (1919) equation. In poroelastic theory, AVO can also be calculated except the fluid term included.

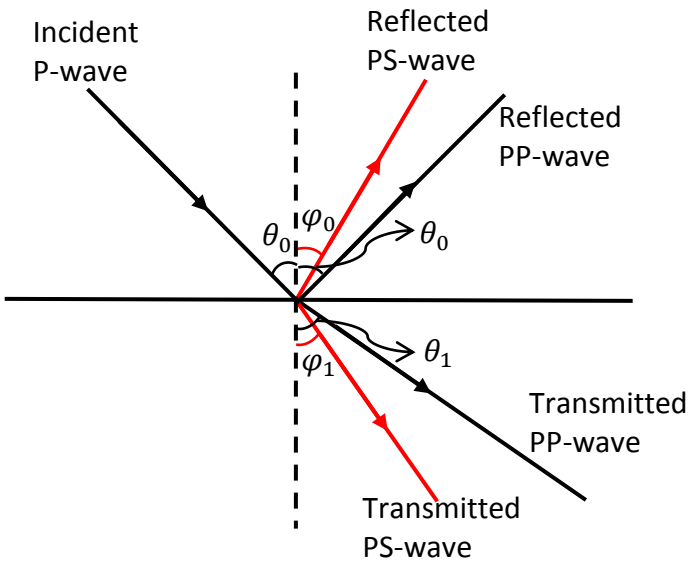

FIG.2. Reflections and transmissions between two elastic media for an incident P-wave

$$\begin{bmatrix} -\sin\theta_0 & -\sqrt{1-\frac{V_{s0}^2}{V_{p0}^2}\sin^2\theta_0} & \frac{V_{p1}}{V_{p0}}\sin\theta_0 & -\sqrt{1-\frac{V_{s1}^2}{V_{p0}^2}\sin^2\theta_0} \\ \sqrt{1-\sin^2\theta_0} & -\frac{V_{s0}}{V_{p0}}\sin\theta_0 & \sqrt{1-\frac{V_{p1}^2}{V_{p0}^2}\sin^2\theta_0} & -\frac{V_{s1}}{V_{p0}}\sin\theta_0 \\ 2\frac{V_{s0}^2}{V_{p0}^2}\sin\theta_0\sqrt{1-\sin^2\theta_0} & \frac{V_{s0}}{V_{p0}}\left[1-2\frac{V_{s0}^2}{V_{p0}^2}\sin^2\theta_0\right] & \frac{2\rho_1}{\rho_0}\frac{V_{s1}^2}{V_{p0}^2}\sin\theta_0\sqrt{1-\frac{V_{p1}^2}{V_{p0}^2}\sin^2\theta_0} & \frac{\rho_1}{\rho_0}\frac{V_{s1}}{V_{p0}}\left[1-2\frac{V_{s1}^2}{V_{p0}^2}\sin^2\theta_0\right] \\ -\left[1-2\frac{V_{s0}^2}{V_{p0}^2}\sin^2\theta_0\right] & 2\frac{V_{s0}^2}{V_{p0}^2}\sin\theta_0\sqrt{1-\frac{V_{s0}^2}{V_{p0}^2}\sin^2\theta_0} & \frac{\rho_1}{\rho_0}\frac{V_{p1}}{V_{p0}}\left[1-2\frac{V_{s1}^2}{V_{p0}^2}\sin^2\theta_0\right] & -\frac{2\rho_1}{\rho_0}\frac{V_{s1}^2}{V_{p0}^2}\sin\theta_0\sqrt{1-\frac{V_{s1}^2}{V_{p0}^2}\sin^2\theta_0} \end{bmatrix} \begin{bmatrix} R_{pp} \\ R_{ps} \\ T_{pp} \\ T_{ps} \end{bmatrix} = \begin{bmatrix} \sin\theta_0 \\ \sqrt{1-\sin^2\theta_0} \\ 2\frac{V_{s0}^2}{V_{p0}^2}\sin\theta_0\sqrt{1-\sin^2\theta_0} \\ 1-2\frac{V_{s0}^2}{V_{p0}^2}\sin^2\theta_0 \end{bmatrix} \quad (12)$$

If we assume perturbation term between two poroelastic media can be calculated by

$$a_M = 1-\frac{M_0}{M_1};\quad a_\mu = 1-\frac{\mu_0}{\mu_1};\quad a_\rho = 1-\frac{\rho_0}{\rho_1}; \qquad (13)$$

Or ratio terms:

$$\frac{\Delta M}{M} = 2\frac{M_1-M_0}{M_1+M_0};\quad \frac{\Delta\mu}{\mu} = 2\frac{\mu_1-\mu_0}{\mu_1+\mu_0};\quad \frac{\Delta\rho}{\rho} = 2\frac{\rho_1-\rho_0}{\rho_1+\rho_0}; \qquad (14)$$

We start from equation (12), redraw each item of coefficient matrix in terms of (a_M , a_μ , a_ρ , γ_{sat} , $\sin\theta_0$) or ($\frac{\Delta M}{M}$, $\frac{\Delta\mu}{\mu}$, $\frac{\Delta\rho}{\rho}$, γ_{sat} , $\sin\theta_0$), and then applying Cramer's rule to generate series expression for R_{pp} and R_{ps} with Maple, then AVO/AVA approximation with P- and S- wave moduli both in perturbation form and ratio form can be derived.

Perturbation form for R_{pp} and R_{ps} (details of 2nd order and 3rd order for R_{pp} and R_{ps} can be found in Appendix I), (state: for writing convenience, all γ_{dry}=$(\frac{V_{p0}}{V_{s0}})_{dry}$ in the following sections represent that the P- and S- wave velocity ratio in the upper layer):

$$R_{pp}^{(1)} = \left(\frac{\sec^2\theta_0}{4}\right)a_M - \left(\frac{2}{\gamma_{sat}^2}\sin^2\theta_0\right)a_\mu + \left(\frac{1}{2} - \frac{\sec^2\theta_0}{4}\right)a_\rho \tag{15}$$

$$R_{pp}^{(2)} = \Gamma_{2M}^{pp}a_M^2 + \Gamma_{2\mu}^{pp}a_\mu^2 + \Gamma_{2\rho}^{pp}a_\rho^2 + \Gamma_{M\rho}^{pp}a_M a_\rho + \Gamma_{\mu\rho}^{pp}a_\mu a_\rho + \Gamma_{M\mu}^{pp}a_M a_\mu \tag{16}$$

$$\begin{aligned} R_{pp}^{(3)} = {} & \Gamma_{3M}^{pp}a_M^3 + \Gamma_{3\mu}^{pp}a_\mu^3 + \Gamma_{3\rho}^{pp}a_\rho^3 + \Gamma_{2\mu\rho}^{pp}a_\mu^2 a_\rho + \Gamma_{2\mu M}^{pp}a_\mu^2 a_M + \Gamma_{\mu 2\rho}^{pp}a_\mu a_\rho^2 \\ & + \Gamma_{\mu 2M}^{pp}a_\mu a_M^2 + \Gamma_{M2\rho}^{pp}a_M a_\rho^2 + \Gamma_{\rho 2M}^{pp}a_\rho a_M^2 + \Gamma_{M\mu\rho}^{pp}a_M a_\mu a_\rho \end{aligned} \tag{17}$$

$$R_{ps}^{(1)} = \left(-\frac{1}{\gamma_{sat}}\sin\theta_0\right)a_\mu + \left(-\frac{1}{2}\sin\theta_0\right)a_\rho \tag{18}$$

$$R_{ps}^{(2)} = \Gamma_{2M}^{ps}a_M^2 + \Gamma_{2\mu}^{ps}a_\mu^2 + \Gamma_{2\rho}^{ps}a_\rho^2 + \Gamma_{M\rho}^{ps}a_M a_\rho + \Gamma_{\mu\rho}^{ps}a_\mu a_\rho + \Gamma_{M\mu}^{ps}a_M a_\mu \tag{19}$$

$$\begin{aligned} R_{ps}^{(3)} = {} & \Gamma_{3M}^{ps}a_M^3 + \Gamma_{3\mu}^{ps}a_\mu^3 + \Gamma_{3\rho}^{ps}a_\rho^3 + \Gamma_{2\mu\rho}^{ps}a_\mu^2 a_\rho + \Gamma_{2\mu M}^{ps}a_\mu^2 a_M + \Gamma_{\mu 2\rho}^{ps}a_\mu a_\rho^2 \\ & + \Gamma_{\mu 2M}^{ps}a_\mu a_M^2 + \Gamma_{M2\rho}^{ps}a_M a_\rho^2 + \Gamma_{\rho 2M}^{ps}a_\rho a_M^2 + \Gamma_{M\mu\rho}^{ps}a_M a_\mu a_\rho \end{aligned} \tag{20}$$

Ratio form for R_{pp} and R_{ps} (details of 2nd order and 3rd order can be found in Appendix II):

$$R_{pp}^{(1)} = \left(\frac{\sec^2\theta_0}{4}\right)\frac{\Delta M}{M} - \left(\frac{2}{\gamma_{sat}^2}\sin^2\theta_0\right)\frac{\Delta\mu}{\mu} + \left(\frac{1}{2} - \frac{\sec^2\theta_0}{4}\right)\frac{\Delta\rho}{\rho} \tag{21}$$

$$\begin{aligned} R_{pp}^{(2)} = {} & \Lambda_{2M}^{pp}\left(\frac{\Delta M}{M}\right)^2 + \Lambda_{2\mu}^{pp}\left(\frac{\Delta\mu}{\mu}\right)^2 + \Lambda_{2\rho}^{pp}\left(\frac{\Delta\rho}{\rho}\right)^2 \\ & + \Lambda_{M\mu}^{pp}\frac{\Delta M}{M}\frac{\Delta\mu}{\mu} + \Lambda_{M\rho}^{pp}\frac{\Delta M}{M}\frac{\Delta\rho}{\rho} + \Lambda_{\mu\rho}^{pp}\frac{\Delta\mu}{\mu}\frac{\Delta\rho}{\rho} \end{aligned} \tag{22}$$

$$\begin{aligned} R_{pp}^{(3)} = {} & \Lambda_{3M}^{pp}\left(\frac{\Delta M}{M}\right)^3 + \Lambda_{3\mu}^{pp}\left(\frac{\Delta\mu}{\mu}\right)^3 + \Lambda_{3\rho}^{pp}\left(\frac{\Delta\rho}{\rho}\right)^3 + \Lambda_{2\mu\rho}^{pp}\left(\frac{\Delta\mu}{\mu}\right)^2\frac{\Delta\rho}{\rho} \\ & + \Lambda_{2\mu M}^{pp}\left(\frac{\Delta\mu}{\mu}\right)^2\frac{\Delta M}{M} + \Lambda_{\mu 2\rho}^{pp}\frac{\Delta\mu}{\mu}\left(\frac{\Delta\rho}{\rho}\right)^2 + \Lambda_{\mu 2M}^{pp}\frac{\Delta\mu}{\mu}\left(\frac{\Delta M}{M}\right)^2 \\ & + \Lambda_{M2\rho}^{pp}\frac{\Delta M}{M}\left(\frac{\Delta\rho}{\rho}\right)^2 + \Lambda_{\rho 2M}^{pp}\frac{\Delta\rho}{\rho}\left(\frac{\Delta M}{M}\right)^2 + \Lambda_{M\mu\rho}^{pp}\frac{\Delta M}{M}\frac{\Delta\mu}{\mu}\frac{\Delta\rho}{\rho} \end{aligned} \tag{23}$$

$$R_{ps}^{(1)} = \left(-\frac{1}{\gamma_{sat}} \sin\theta_0 \right) \frac{\Delta\mu}{\mu} + \left(-\frac{1}{2} \sin\theta_0 \right) \frac{\Delta\rho}{\rho} \tag{24}$$

$$\begin{aligned} R_{ps}^{(2)} = {} & \Lambda_{2M}^{ps} \left(\frac{\Delta M}{M} \right)^2 + \Lambda_{2\mu}^{ps} \left(\frac{\Delta\mu}{\mu} \right)^2 + \Lambda_{2\rho}^{ps} \left(\frac{\Delta\rho}{\rho} \right)^2 \\ & + \Lambda_{M\mu}^{ps} \frac{\Delta M}{M} \frac{\Delta\mu}{\mu} + \Lambda_{M\rho}^{ps} \frac{\Delta M}{M} \frac{\Delta\rho}{\rho} + \Lambda_{\mu\rho}^{ps} \frac{\Delta\mu}{\mu} \frac{\Delta\rho}{\rho} \end{aligned} \tag{25}$$

$$\begin{aligned} R_{ps}^{(3)} = {} & \Lambda_{3M}^{ps} \left(\frac{\Delta M}{M} \right)^3 + \Lambda_{3\mu}^{ps} \left(\frac{\Delta\mu}{\mu} \right)^3 + \Lambda_{3\rho}^{ps} \left(\frac{\Delta\rho}{\rho} \right)^3 + \Lambda_{2\mu\rho}^{ps} \left(\frac{\Delta\mu}{\mu} \right)^2 \frac{\Delta\rho}{\rho} \\ & + \Lambda_{2\mu M}^{ps} \left(\frac{\Delta\mu}{\mu} \right)^2 \frac{\Delta M}{M} + \Lambda_{\mu 2\rho}^{ps} \frac{\Delta\mu}{\mu} \left(\frac{\Delta\rho}{\rho} \right)^2 + \Lambda_{\mu 2M}^{ps} \frac{\Delta\mu}{\mu} \left(\frac{\Delta M}{M} \right)^2 \\ & + \Lambda_{M2\rho}^{ps} \frac{\Delta M}{M} \left(\frac{\Delta\rho}{\rho} \right)^2 + \Lambda_{\rho 2M}^{ps} \frac{\Delta\rho}{\rho} \left(\frac{\Delta M}{M} \right)^2 + \Lambda_{M\mu\rho}^{ps} \frac{\Delta M}{M} \frac{\Delta\mu}{\mu} \frac{\Delta\rho}{\rho} \end{aligned} \tag{26}$$

where $R_{pp}^{(1)}, R_{pp}^{(2)}, R_{pp}^{(3)}$ of equations (15)-(26) are the 1st, 2nd ,3rd orders in R_{pp}, respectively, both for perturbation form and ratio form.

To take a glance at the influence of high order term of R_{pp}, R_{ps} and the accuracy of the new AVO approximation both in perturbation form and in ratio form, we compared each truncated term with the exact solution of R_{pp} obtained from Zoeppritz equation on a slight change fluid-saturated rock with angle incidence start from 0 to 90 degrees. The parameters P-wave velocity, S-wave velocity and density [V_p, V_s, ρ] in upper media are [2857m/s, 1666m/s, 2275kg/m3], for lower media, parameters of saturated rock are [2898m/s, 1290m/s, 2425kg/m3]. In Figure 3, we focus on the high order effect of R_{pp}, in perturbation form. After comparison of each truncated term to exact solution, we can observe that, the accuracy increase when high order included in R_{pp} especially for small incidence angle, but 3rd truncated order might disperse at large angle, around 70 to 75 degree, compared to 2nd order. However, overall 3rd truncated term of R_{pp}, has a better accuracy than 1st and 2nd truncated order. Figure 4 shows the comparison of R_{ps}, in perturbation form, after analysis, 2nd truncated order would be a sensible choice to do the converted AVO analysis of this media.

In Figure 5, the comparison of R_{pp}, in ratio form was discussed, 2nd truncated and 3rd truncated R_{pp} have a better resolution than linear approximation, but there is not too much improvement of 3rd truncated order compared to 2nd truncated order. We believe 2nd truncated R_{pp} will be a wise choice after the computational burden considered. Figure 6 indicates the comparison of R_{ps} in ratio form with angle incidence, and 2nd truncated order was also the result with the highest resolution.

Figure 7 also indicates that the comparison of R_{pp}, in ratio form, but the angle incidence of the formula is replaced by the average angle which is defined as the average value of incident and refracted plane wave angles at the boundary. and it can be observed that 2nd and 3rd truncated order also have a better solution than 1st linear approximation,

improvement of 3rd truncated order is inconspicuous, 2nd truncated order is a advisable choice for AVO analysis. We do the same substitution between angle incidence and average angle in Figure 8 for R_{ps}, 2nd truncated R_{ps} has the best precision compared to 1st and 3rd truncated order.

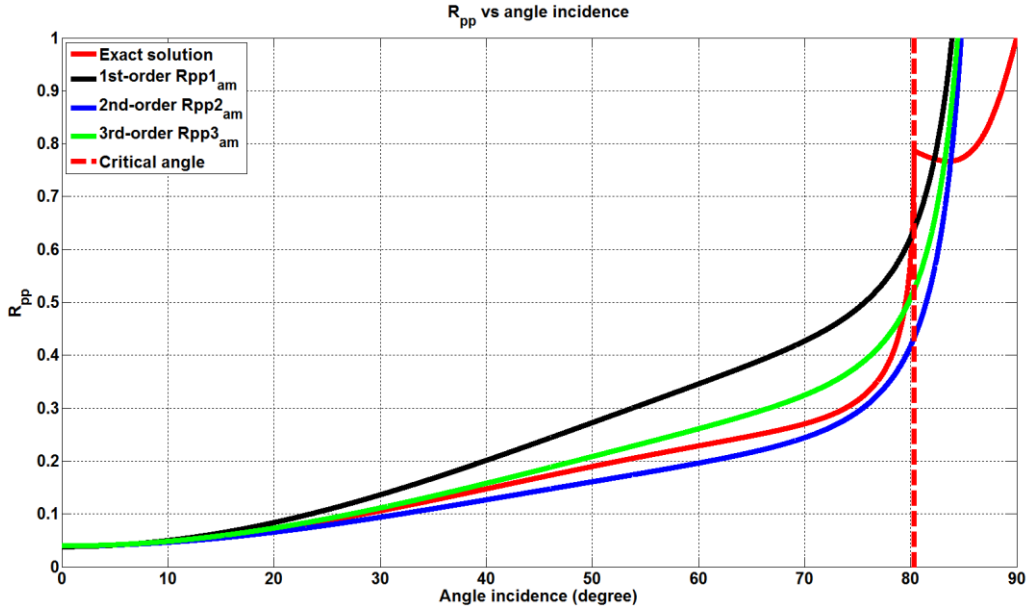

FIG.3. Comparison of R_{pp}, with 1st, 2nd, 3rd, orders in perturbation form. The exact solution for R_{pp} calculated using Zoeppritz equation is indicated in red, the 1st order (linear approximation) solution is indicated in black, the 2nd truncated order of R_{pp}, (includes 1st + 2nd order terms) is indicated in blue, the 3rd truncated order R_{pp}, (1st +2nd +3rd order terms) is indicated in green. Critical angle is delineated in dashed red line.

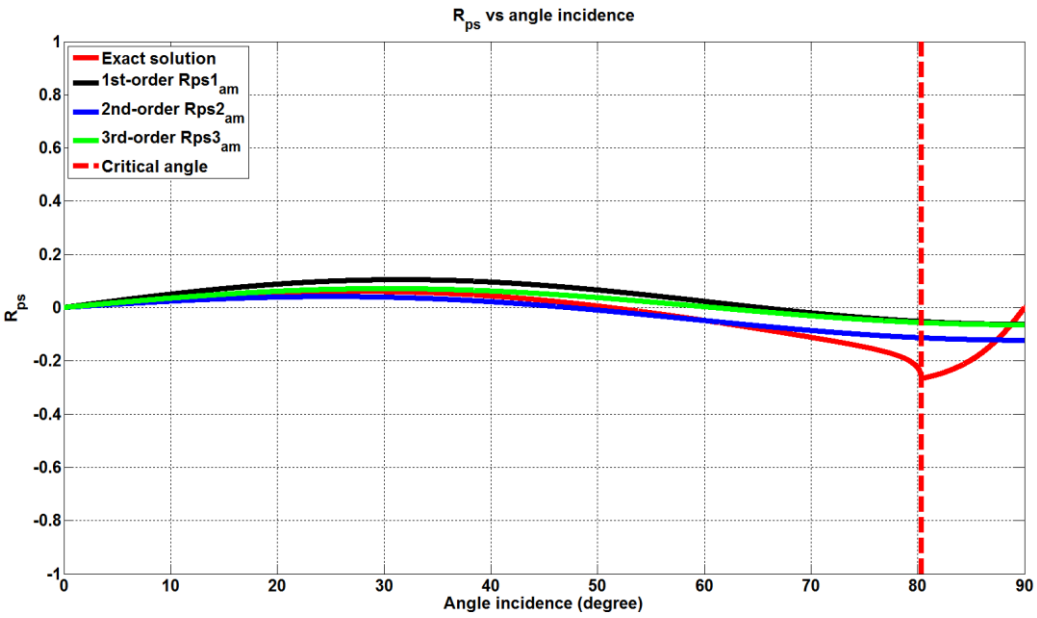

FIG.4. Comparison of $R_{ps}$with 1st, 2nd, 3rd, orders in perturbation form. The exact solution for R_{ps} calculated using Zoeppritz equation is indicated in red, the 1st order (linear approximation)

solution is indicated in black, the 2nd truncated order of R_{ps}, (includes 1st + 2nd order terms) is indicated in blue, the 3rd truncated order R_{ps} (1st +2nd +3rd order terms) is indicated in green. And the critical angle labelled is for reflected PP-wave.

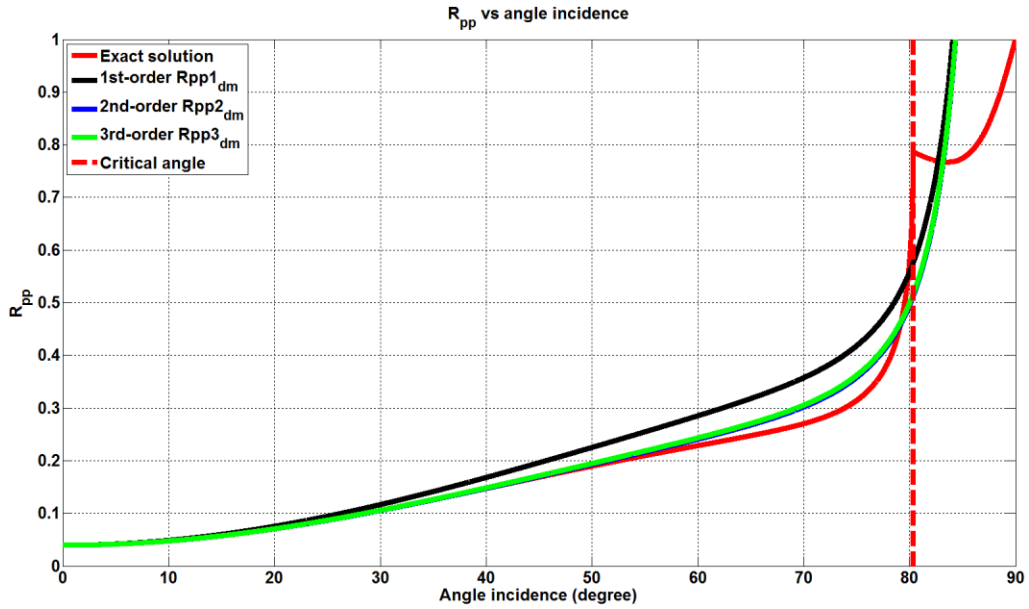

FIG.5. Comparison of R_{pp} with 1st, 2nd, 3rd, orders in ratio form. The exact solution for R_{pp} calculated using Zoeppritz equation is indicated in red, the 1st order (linear approximation) solution is indicated in black, the 2nd truncated order of R_{pp} (includes 1st + 2nd order terms) is indicated in blue, the 3rd truncated order R_{pp} (1st +2nd +3rd order terms) is indicated in green. Critical angle is delineated in dashed red line.

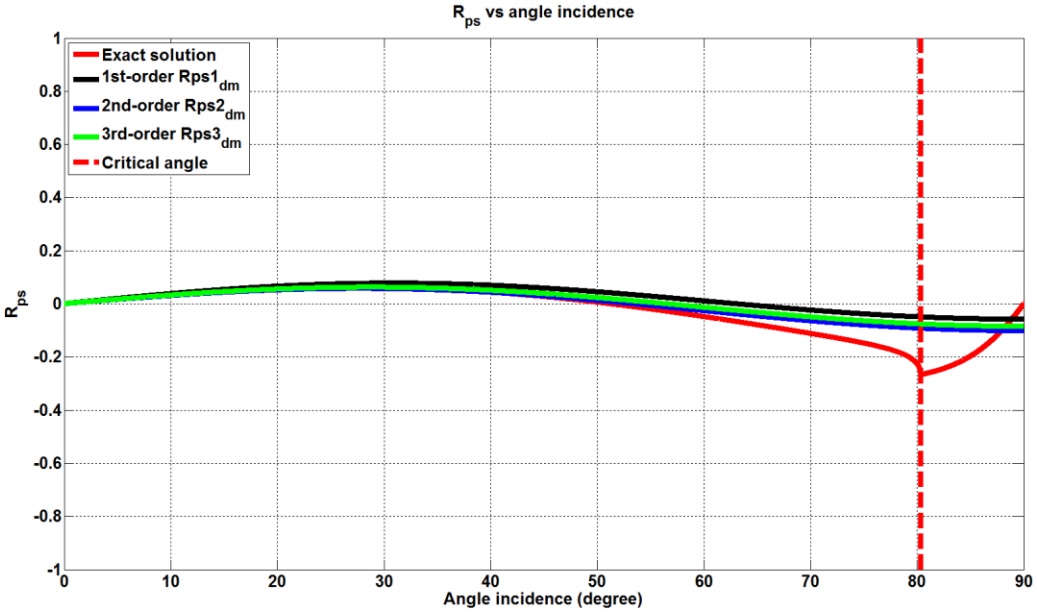

FIG.6. Comparison of R_{ps} with 1st, 2nd, 3rd, orders in ratio form. The exact solution for R_{ps} calculated using Zoeppritz equation is indicated in red, the 1st order (linear approximation) solution is indicated in black, the 2nd truncated order of R_{ps} (includes 1st + 2nd order terms) is

indicated in blue, the 3rd truncated order R_{ps} (1st +2nd +3rd order terms) is indicated in green. And the critical angle labelled is for reflected PP-wave.

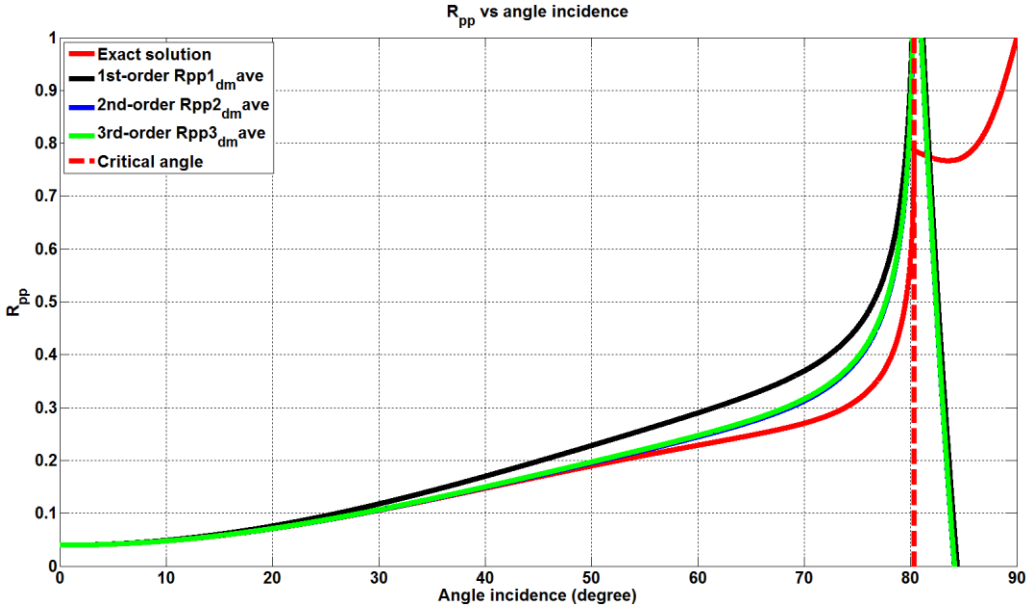

FIG.7. Comparison of R_{pp} with 1st, 2nd, 3rd, orders in ratio form, but angle represent the average of the incident and the refracted angles. The exact solution for R_{pp} calculated using Zoeppritz equation is indicated in red, the 1st order (linear approximation) solution is indicated in black, the 2nd truncated order of R_{pp} (includes 1st + 2nd order terms) is indicated in blue, the 3rd truncated order R_{pp} (1st +2nd +3rd order terms) is indicated in green. Critical angle is delineated in dashed red line.

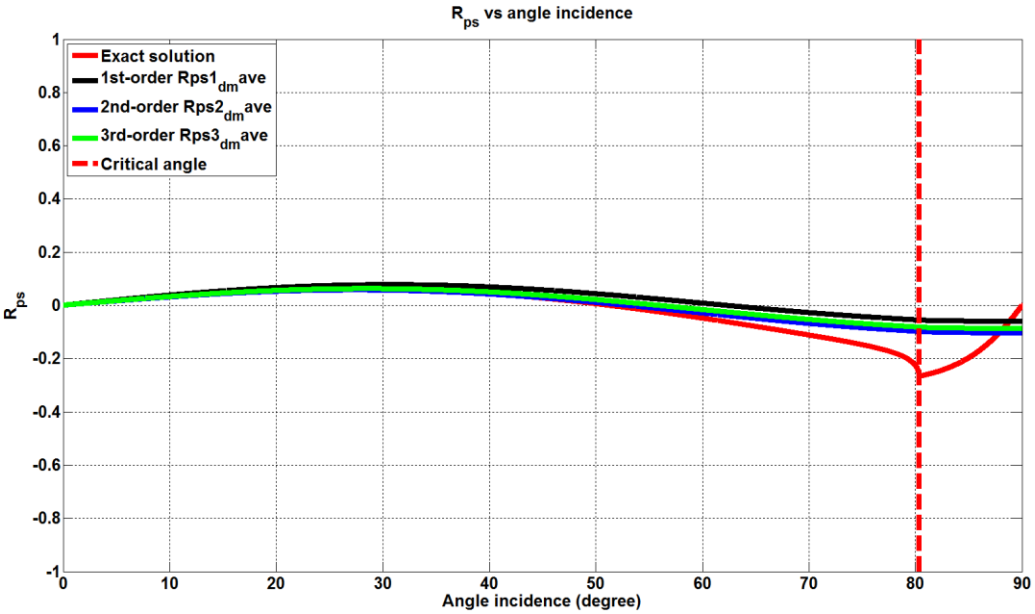

FIG.8. Comparison of R_{ps} with 1st, 2nd, 3rd, orders in ratio form, but angle represent the average of the incident and the refracted angles. The exact solution for R_{ps} calculated using Zoeppritz equation is indicated in red, the 1st order (linear approximation) solution is indicated in black, the 2nd truncated order of R_{ps} (includes 1st + 2nd order terms) is indicated in blue, the 3rd truncated

order R_{ps} (1st +2nd +3rd order terms) is indicated in green. And the critical angle labelled is for reflected PP-wave.

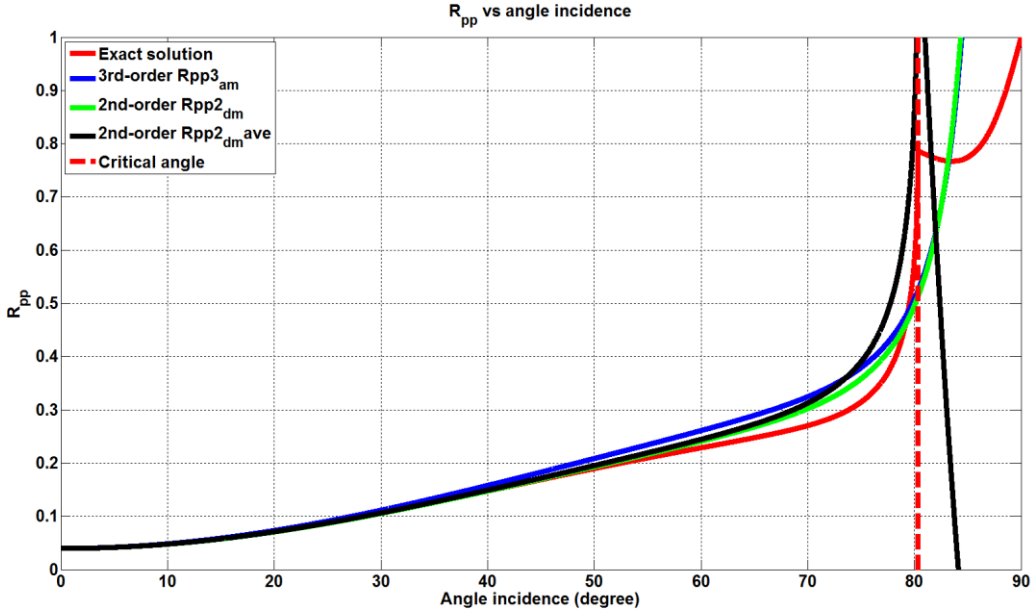

FIG.9. Comparison of R_{pp} both in perturbation and ratio form and with average angle. The exact solution for R_{pp} calculated using Zoeppritz equation is indicated in red, the truncated 3rd order R_{pp} in perturbation form is indicated in blue, the 2nd truncated order of R_{pp} with indigence angle in ratio form is indicated in green, and the 2nd truncated order of R_{pp} with average angle is indicated in black. Critical angle is delineated in dashed red line.

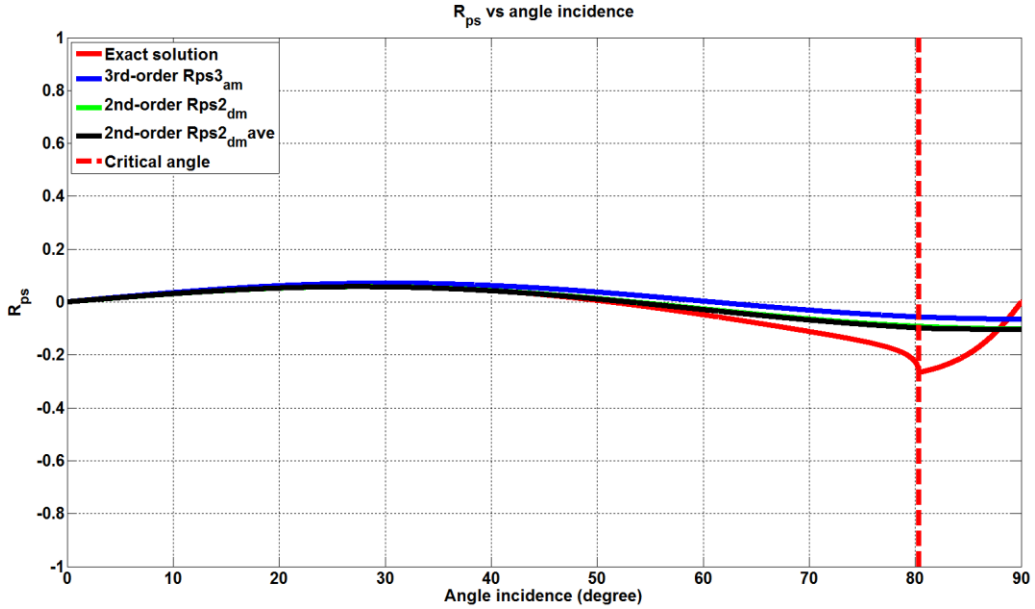

FIG.10. Comparison of R_{ps} both in perturbation and ratio form and with average angle. The exact solution for R_{ps} calculated using Zoeppritz equation is indicated in red, the truncated 3rd order R_{ps} in perturbation form is indicated in blue, the 2nd truncated order of R_{ps} with indigence angle in ratio form is indicated in green, and the 2nd truncated order of R_{ps} with average angle is indicated in black. Critical angle for reflected PP wave is delineated in dashed red line.

The discussions of the high order effect of R indicate that, 3rd truncated R_{pp} in perturbation form, 2nd truncated R_{pp} in ratio form, 2nd truncated R_{pp} with average angle in ratio form have a relative better resolution. And we compared them in Figure 9, all of them have a great resolution when angle incidence is less than 50 degree, and 2nd truncated R_{pp} in ratio form has a better resolution with incidence angle increasing after 50 degree. In Figure 10, a similar comparison was done among the related R_{ps} corresponding to R_{pp} of Figure 9, two approximations in ratio form have a better resolution than 3rd truncated R_{ps} in perturbation form, and there are not too much difference between two approximations in ratio form.

In the end of this section, with consideration of the accuracy of R_{pp}, the 2nd truncated R_{pp} with incidence angle in ratio form will be considered as the AVO approximation formula to achieve non-linear AVO/AVA inversion with a combination of series reversion and Gauss-Newton iteration in the experiment.

NON-LINEAR AVO/AVA INVERSION

Based on the precious discussions, non-linear AVO approximation is prepared for inversion. The next step is how to connect those approximations with series reversion and Gauss-Newton iteration. From this moment on, only approximation of PP-wave R_{pp} will be considered as an example to show the connections.

AVO/AVA series reversion

Consider the connection of series reversion and AVO/AVA, the reflection coefficient is the function of petrophysical parameters, in here, R_{pp} can be expressed as the function of $\Delta M/M$, $\Delta\mu/\mu$ and $\Delta\rho/\rho$. Therefore, R_{pp} can also be expanded as a series, written as

$$R_{pp} = R_{pp}^{(1)} + R_{pp}^{(2)} + R_{pp}^{(3)} + \cdots; \tag{27}$$

where, $R_{pp}^{(1)}, R_{pp}^{(2)}, R_{pp}^{(3)}$ are 1st , 2nd , 3rd orders in series expansion of R_{pp}, and they can be expressed as

$$R_{pp}^{(1)} = A_1 d_M + B_1 d_\mu + C_1 d_\rho; \tag{28}$$

$$R_{pp}^{(2)} = A_2 d_M^2 + B_2 d_\mu^2 + C_2 d_\rho^2 + D_{M\mu} d_M d_\mu + D_{M\rho} d_M d_\rho + D_{\mu\rho} d_\mu d_\rho; \tag{29}$$

$$\begin{aligned} R_{pp}^{(3)} = {} & A_3 d_M^3 + B_3 d_\mu^3 + C_3 d_\rho^3 + D_{2M\mu} d_M^2 d_\mu + D_{M2\mu} d_M d_\mu^2 + D_{2M\rho} d_M^2 d_\rho \\ & + D_{M2\rho} d_M d_\rho^2 + D_{2\mu\rho} d_\mu^2 d_\rho + D_{\mu 2\rho} d_\mu d_\rho^2 + D_{M\mu\rho} d_M d_\mu d_\rho; \end{aligned} \tag{30}$$

while $d_M = \Delta M/M$, $d_\mu = \Delta\mu/\mu$, $d_\rho = \Delta\rho/\rho$.

In this paper, only first two orders will be considered to non-linear AVO/AVA analysis depending on the discussion above about the accuracy of R_{pp} and R_{ps} in last section. Therefore, R_{pp} can be written as

$$R_{pp} = R_{pp}^{(1)} + R_{pp}^{(2)} = A_1 d_M + B_1 d_\mu + C_1 d_\rho + A_2 d_M^2 + B_2 d_\mu^2 + C_2 d_\rho^2 + D_{M\mu} d_M d_\mu + D_{M\rho} d_M d_\rho + D_{\mu\rho} d_\mu d_\rho; \quad (31)$$

Equation (31) is considered as the definitive formula to non-linear AVO/AVA inversion related to the next sub chapter.

AVO/AVA iteration with Gauss-Newton

The Gauss-Newton algorithm is a classic way to solve non-linear least square problem, typically expressed mathematically as:

$$F = \sum_{i=1}^{N} r_i^2 \quad (32)$$

where F is the objective function, namely, it's the sum of the square of the residuals for all angles. The residual, r_i is the difference between the observed value and the valued estimated by the method,

$$r_i = \varphi_i - s_i \quad (33)$$

while s_i is the actual value we observed, φ_i is the value we predicted using the following formula,

$$\varphi_i = A_1 d_M + B_1 d_\mu + C_1 d_\rho + A_2 d_M^2 + B_2 d_\mu^2 + C_2 d_\rho^2 + D_{M\mu} d_M d_\mu + D_{M\rho} d_M d_\rho + D_{\mu\rho} d_\mu d_\rho; \quad (34)$$

Then the i-th iterative step can be expressed as

$$x_{i+1} = x_i - H_i^{-1} \overrightarrow{g_i} \quad (35)$$

In here, x_{i+1} is the parameter vector we yearn for, x_i is the input for i-th iterative step, H_i^{-1} is the Hessian matrix of the objective function in i-th step, $\overrightarrow{g_i}$ is the gradient of the objective function in i-th step, they can be calculated by

$$x_i = \left[\left(\frac{\Delta M}{M} \right)_i \quad \left(\frac{\Delta \mu}{\mu} \right)_i \quad \left(\frac{\Delta \rho}{\rho} \right)_i \right]^T \quad (36)$$

$$g = \begin{bmatrix} \frac{\partial F}{\partial d_M} \\ \frac{\partial F}{\partial d_\mu} \\ \frac{\partial F}{\partial d_\rho} \end{bmatrix}; \quad (37)$$

$$H=\begin{bmatrix} \dfrac{\partial^2 F}{\partial d_M^2} & \dfrac{\partial^2 F}{\partial d_M \partial d_\mu} & \dfrac{\partial^2 F}{\partial d_M \partial d_\rho} \\ \dfrac{\partial^2 F}{\partial d_\mu \partial d_M} & \dfrac{\partial^2 F}{\partial d_\mu^2} & \dfrac{\partial^2 F}{\partial d_\mu \partial d_\rho} \\ \dfrac{\partial^2 F}{\partial d_\rho \partial d_M} & \dfrac{\partial^2 F}{\partial d_\rho \partial d_\mu} & \dfrac{\partial^2 F}{\partial d_\rho^2} \end{bmatrix} \tag{38}$$

One of the problems of the Gauss-Newton iteration is local convergence, the key point of that is how to choose a proper initial value for iteration. To solve that, or to find an advisable initial value, we back to the series reversion.

$$R_{pp}=R_{pp}^{(1)}+R_{pp}^{(2)}+R_{pp}^{(3)}+\cdots; \tag{39}$$

The idea of solving series reversion is equating both sides of equation (39) like orders after series expansion, and then we have,

$$\begin{cases} R_{pp}=R_{pp}^{(1)} \\ 0=R_{pp}^{(2)} \\ 0=R_{pp}^{(3)} \\ \cdots \end{cases} \tag{40}$$

The first equation in equations (40) is a linear equation, also can be written as

$$\begin{cases} A_1(\theta_1)d_M+B_1(\theta_1)d_\mu+C_1(\theta_1)d_\rho=R_{pp}(\theta_1) \\ A_1(\theta_2)d_M+B_1(\theta_2)d_\mu+C_1(\theta_2)d_\rho=R_{pp}(\theta_2) \\ \cdots \\ A_1(\theta_N)d_M+B_1(\theta_N)d_\mu+C_1(\theta_N)d_\rho=R_{pp}(\theta_N) \end{cases} \tag{41}$$

Linear solution can be easily obtained by solving equation (41), and we will consider this linear solution as the initial value for non-linear Gauss-Newton iterative AVO/AVA inversion.

EXPERIMENT WITH WELL-LOG SYNTHETIC

Synthetic with well-log

Well 12-27 is the log data collected by CREWES at Hussar, Alberta in September, 2011 for low-frequency seismic study, which includes P-wave sonic log, S-wave sonic log, and density log (Figure 11). And V_P/V_S ratio at the well location can be acquired. As indicated, the interested time zone starts from 0.69s to 0.73s. Beyond that, P-wave modulus and S-wave modulus were also calculated at the well location, which is shown in the Figure 12. Then, the variation of P-wave modulus, S-wave modulus, and density can be obtained as well by implemented Eq. (14) (shown in Figure 13), and these will be considered as the exact value and compared to the inversed solution after AVO inversion applied.

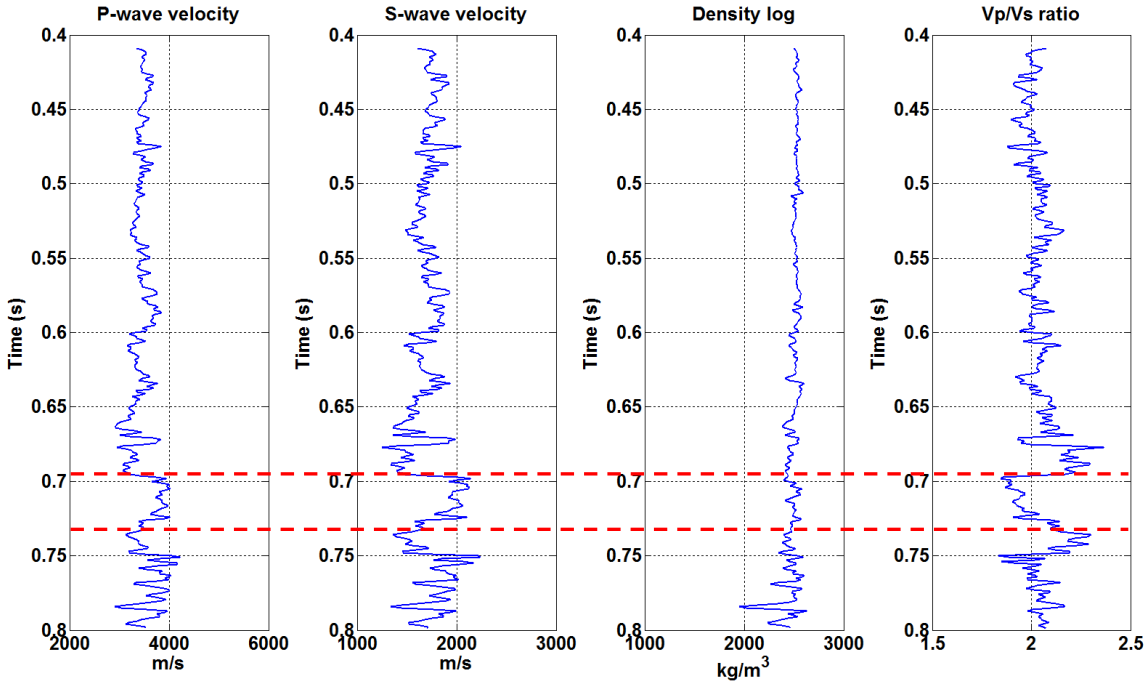

FIG.11. Well 12-27 collected by CREWES in September 2011 at Hussar, Alberta. And P-wave velocity, S-wave velocity, density log, and Vp/Vs ratio are shown from left to right, respectively.

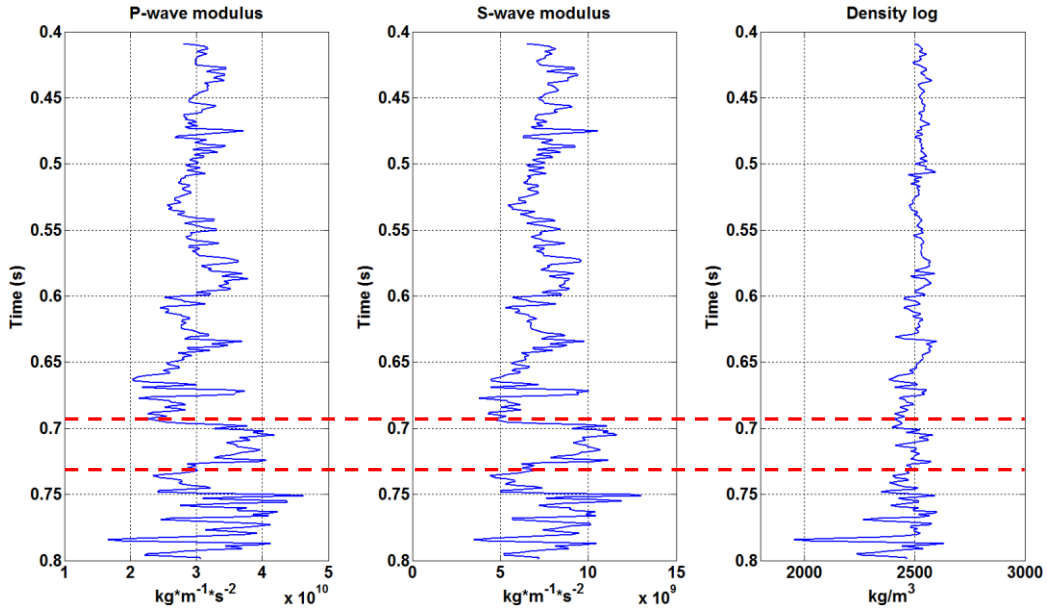

FIG.12. The obtained P-wave modulus, S-wave modulus, and density log at well location.

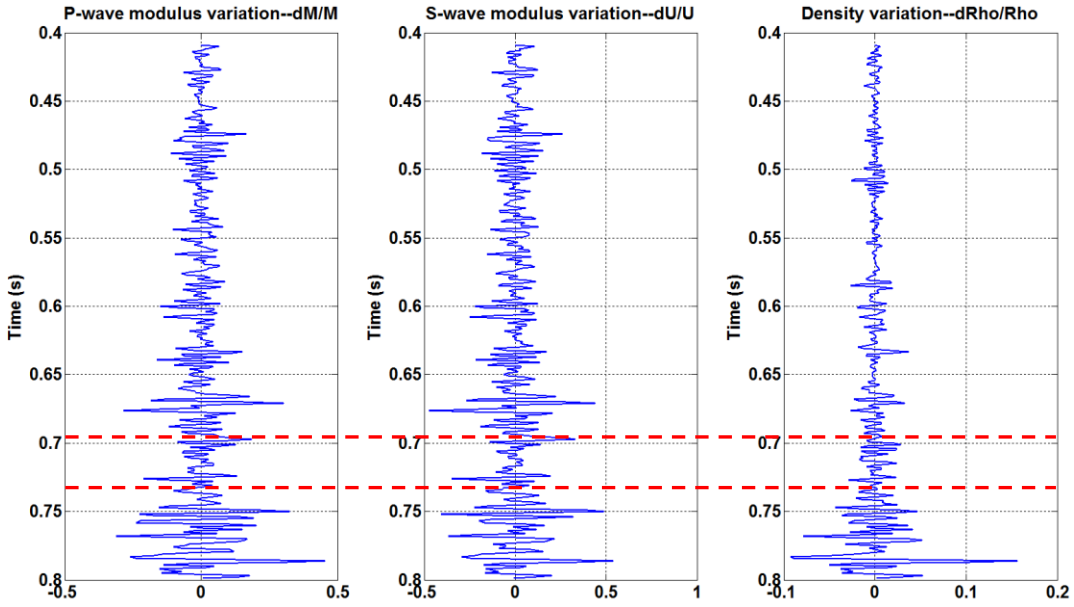

FIG.13. The variation of P-wave modulus, S-wave modulus, and density at well location.

Consider those parameters from well 12-27 as the input of Zoeppritz equation, AVO modelling for PP-wave and PS-wave were achieved by convolving with a min-phase wavelet. Both PP-wave modelling and PS-wave modelling datasets are arranged in incidence angle from 0 to 50 degrees, and are shown in Figure 14 and 15 respectively. These will be applied to examine the accuracy of the non-linear AVO/AVA inversion with a combination of series reversion and Gauss-Newton iteration.

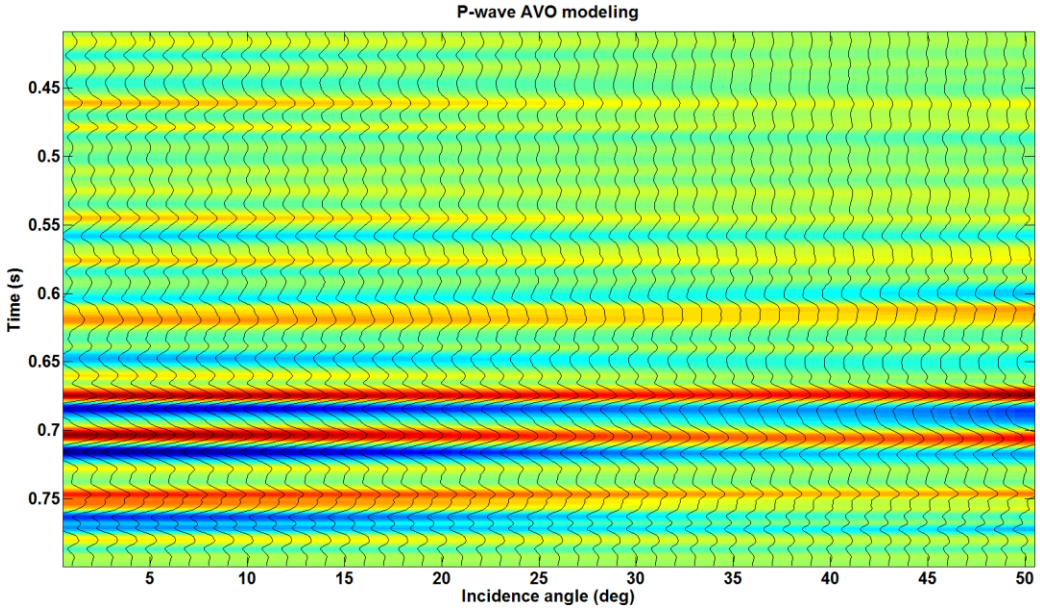

FIG. 14. The angle gather of PP-wave modeling using Zoeppritz equation from 0 to 50 degrees.

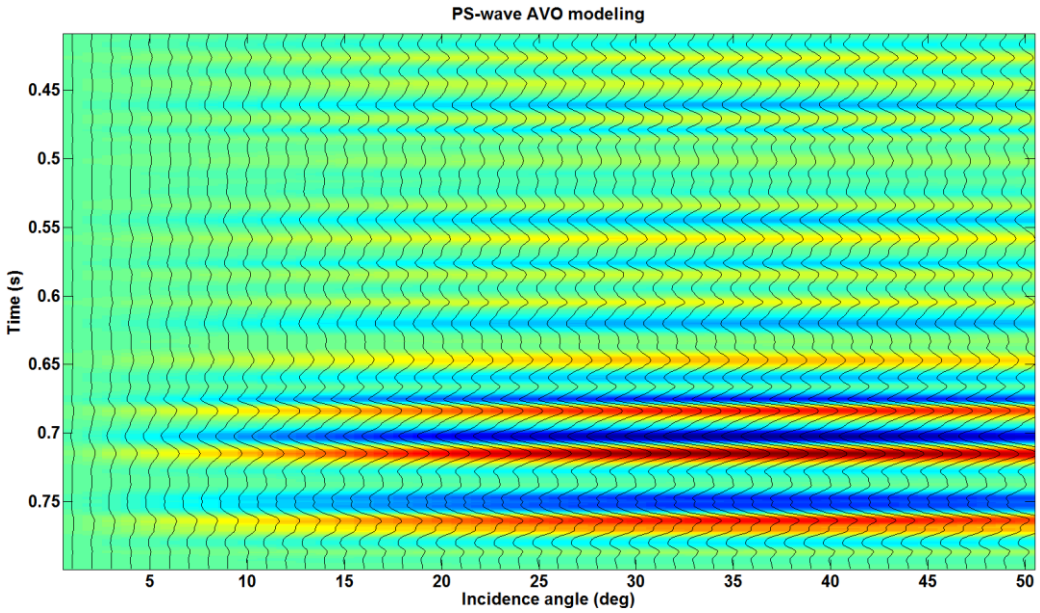

FIG. 15. The angle gather of PS-wave modeling using Zoeppritz equation from 0 to 50 degrees.

AVO inversion with PP-wave modelling

AVO synthetic modeling with well-log for PP-wave (Figure 14) will be applied to the non-linear AVO inversion we stated in precious section. To examine how well the nonlinear AVO inversion algorithm does, we also implemented a linear AVO inversion and compared the results from non-linear AVO inversion with the linear inversed results.

Figure 16 and Figure 17 show us the linear inversed results and the results using non-linear inversion for density, P- and S- wave modulus, respectively, and both of them are compared with well-log data. Figure 18 shows the comparison between linear and non-linear approach in a zoomed in scale. As we can see, linear results matched with well-log data to some extent, but we still have some mismatched points. Compared to that, non-linear results shows a great agreement with well log data, even extremely perfect results in P-wave modulus and density. And to inspect the accuracy of this non-linear AVO/AVA method and get a better review of those comparisons, estimated errors of all inversed results are calculated, both for linear inversion and non-linear inversion.

Figure 19 and 20 indicated the inversed errors of P-, S-wave modulus, and density in the same scale, using linear inversion and nonlinear inversion we proposed, respectively. Both of linear and non-linear inversion acquired quite matched results for P-wave modulus and density, and nonlinear inversed results are still better than linear inversed results. For S-wave modulus, the errors using linear method are not even acceptable while the nonlinear algorithm achieved much better results with no more than 7 iterations. Therefore, in this case, the nonlinear AVO inversion with a combination of series reversion and Gauss-Newton using PP-wave data is an efficient and better choice compared with linear inversion.

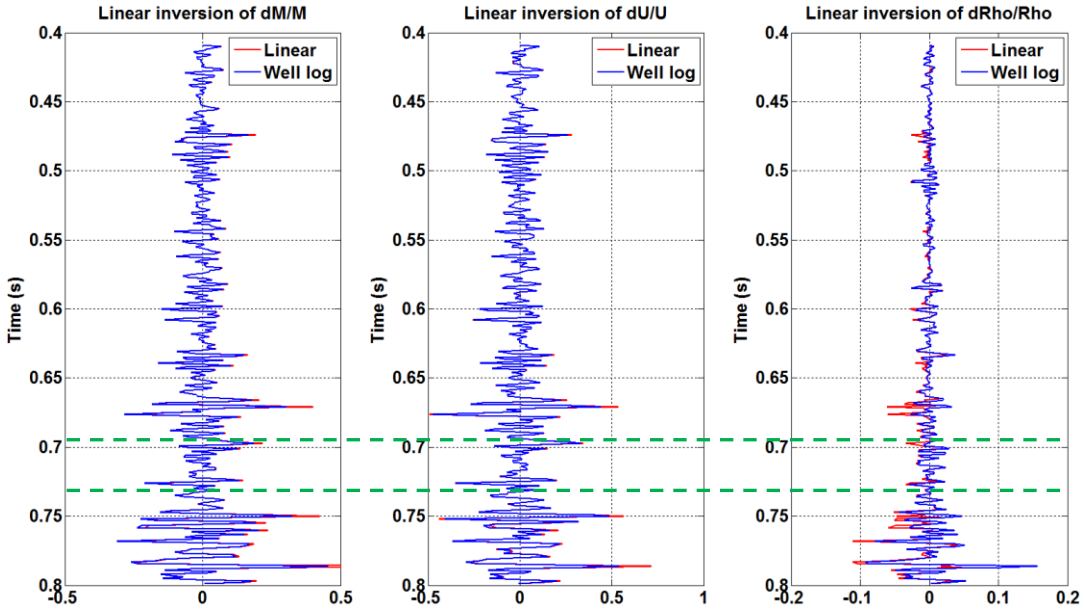

FIG. 16. The comparison between linear AVO results (using PP-wave modelling data) and well-log for the variation of P-wave modulus, S-wave modulus, and density, from left to right.

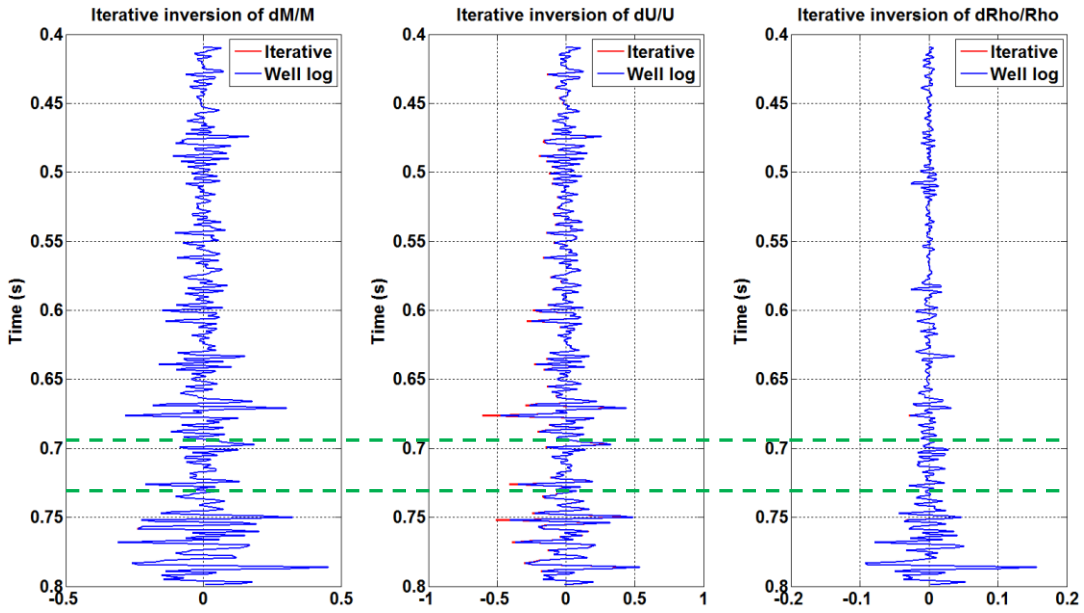

FIG. 17. The comparison between non-linear AVO results (using PP-wave modelling data) and well-log for the variation of P-wave modulus, S-wave modulus, and density, from left to right.

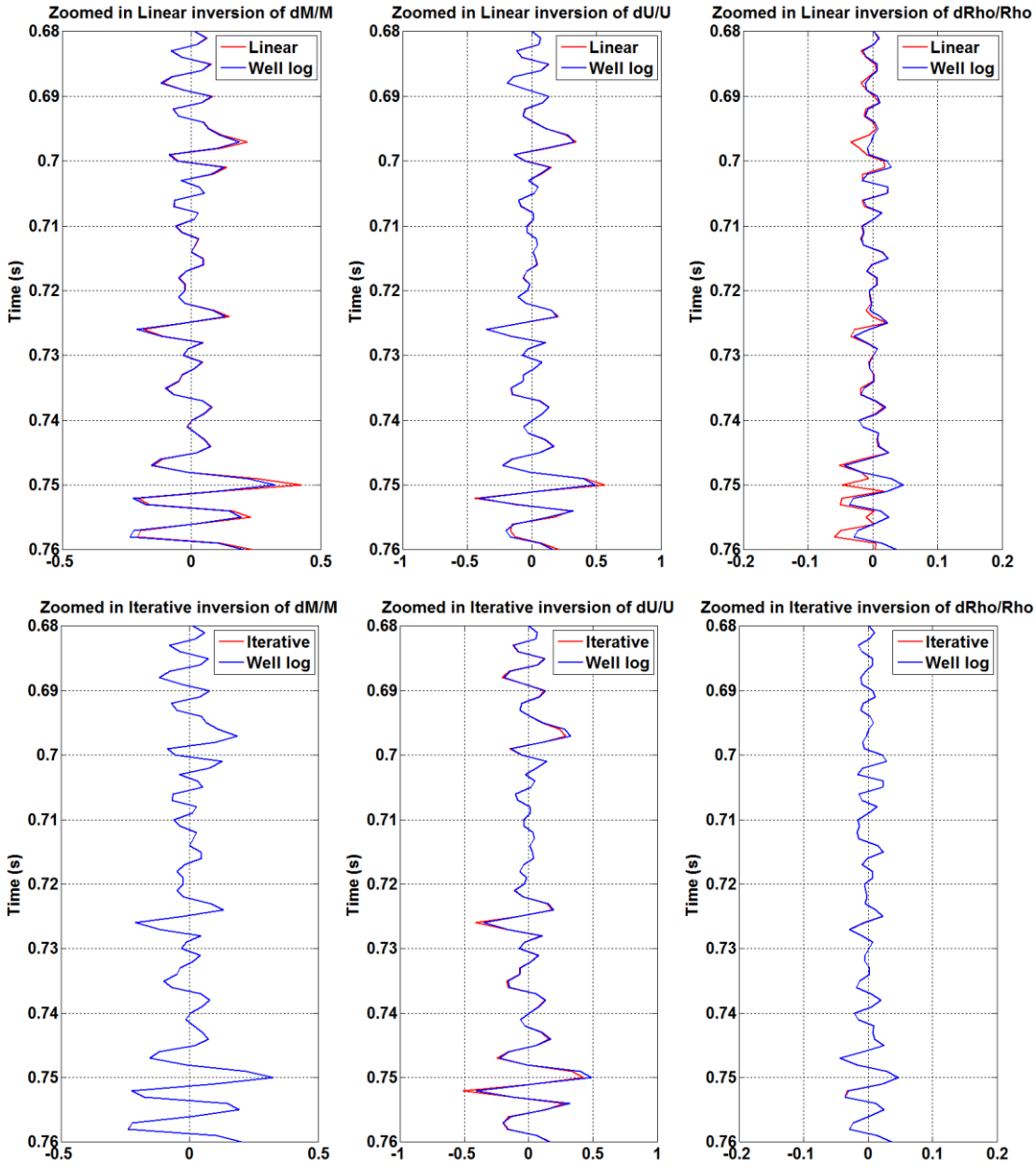

FIG. 18. The comparison between linear inversed results and non-linear AVO inversions for the variation of P-wave modulus, S-wave modulus, and density, using PP-wave modelling data. The upper and lower panel show Figure 16 and 17 in a zoomed in scale, respectively.

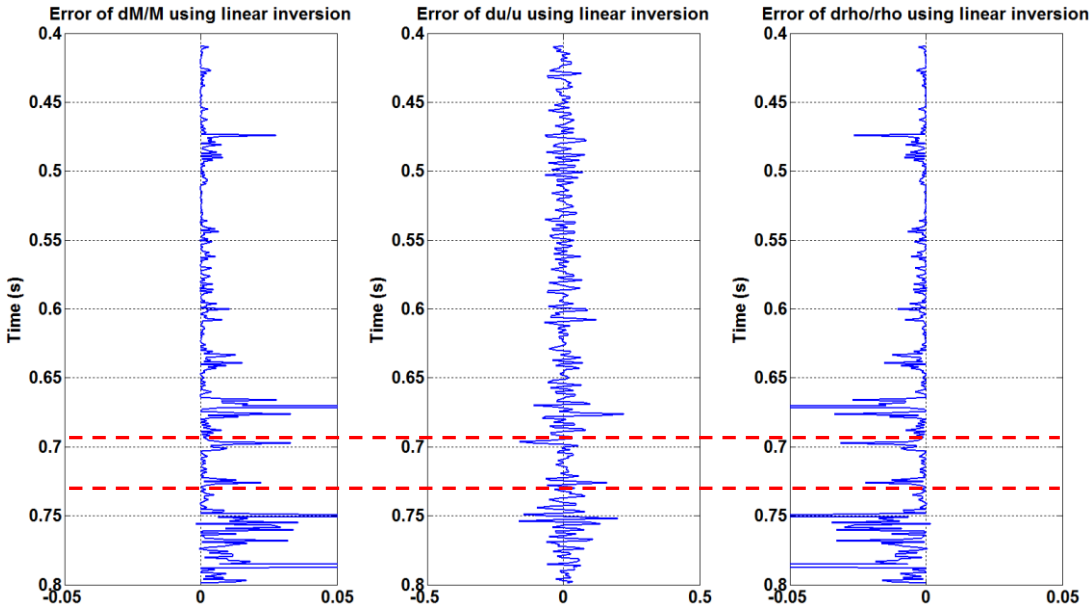

FIG. 19. Errors of inversed P-, S-wave modus, and density using linear inversion with PP-wave modelling data.

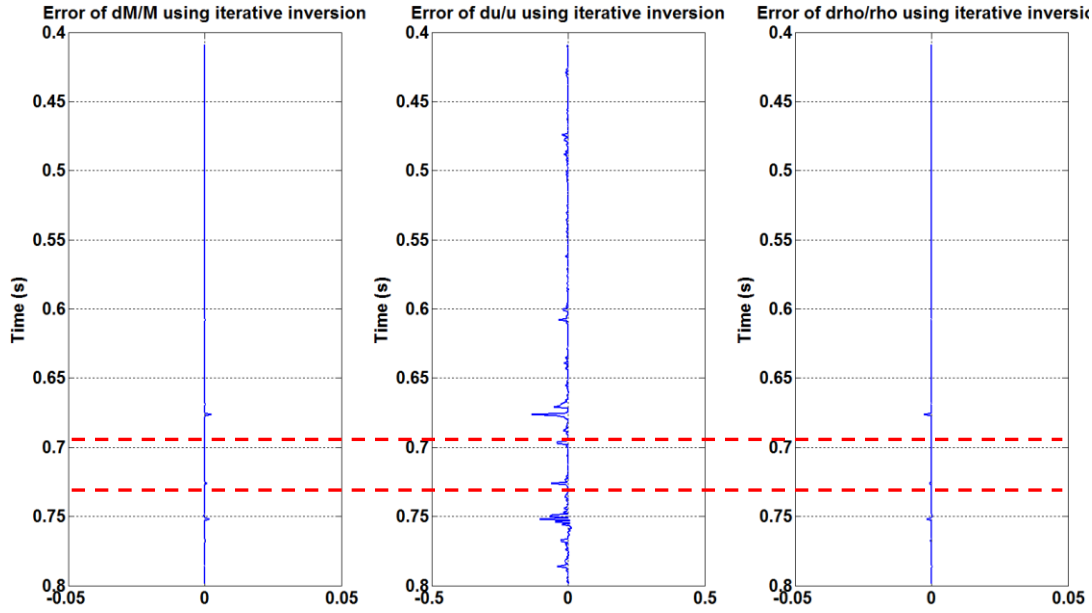

FIG. 20. Errors of inversed P-, S-wave modus, and density using non-linear AVO inversion with a combination of series reversion and Gauss-Newton with PP-wave modelling data.

AVO inversion with PS-wave modelling

In this section, PS-wave synthetic data we generated using Zoeppritz equation will be considered as an input of converted wave AVO inversion by implementing the PS-wave version of equation (31). Similarly, the linear inversion is also applied to compare with the nonlinear AVO algorithm.

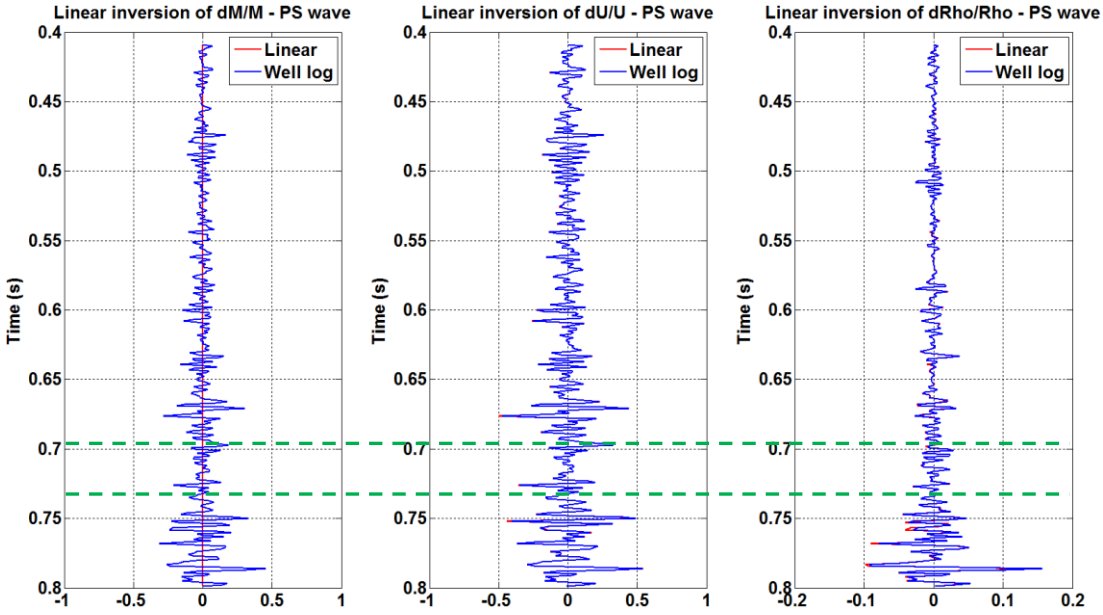

FIG. 21. The comparison between linear AVO results (using PS-wave modelling data) and well-log for the variation of P-wave modulus, S-wave modulus, and density, from left to right.

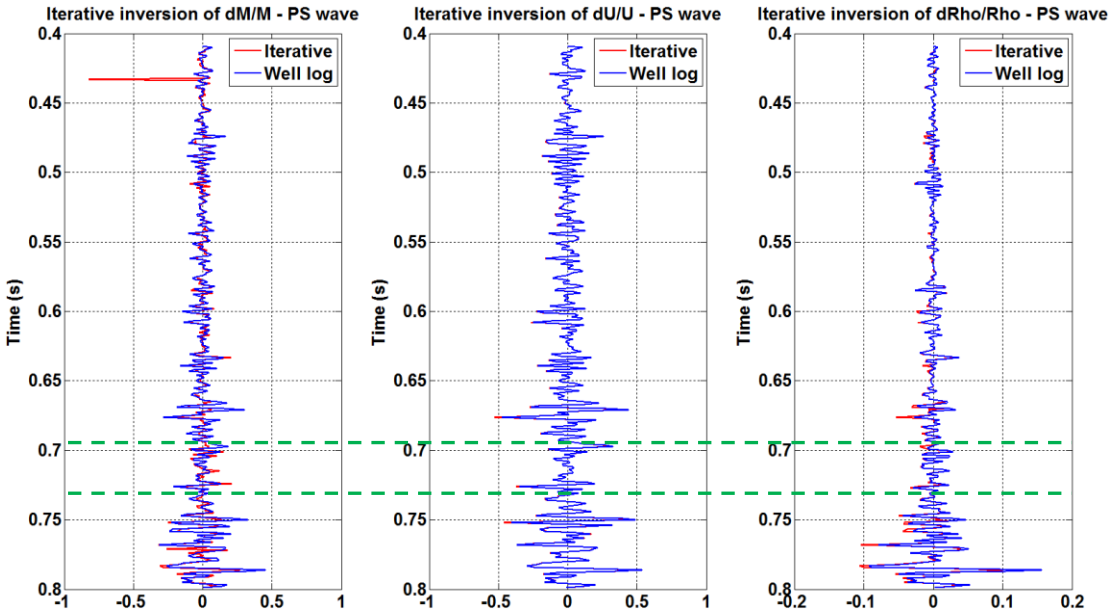

FIG. 22. The comparison between non-linear AVO results (using PS-wave modelling data) and well-log for the variation of P-wave modulus, S-wave modulus, and density, from left to right.

The linear inversion results are indicated in Figure 21, and the estimates of P-wave modulus is zero because of no P-wave modulus term included in the first order terms of R_{ps}. And Figure 22 shows the inversed results using non-linear AVO. Instead of zero-estimated in P-wave modulus using linear algorithm, P-wave modulus can be estimated by the non-linear AVO using PS-wave data. And the variations in the results of P-wave modulus shows an agreement with well-log data to some extent which might still bring some benefits only with PS-wave data.

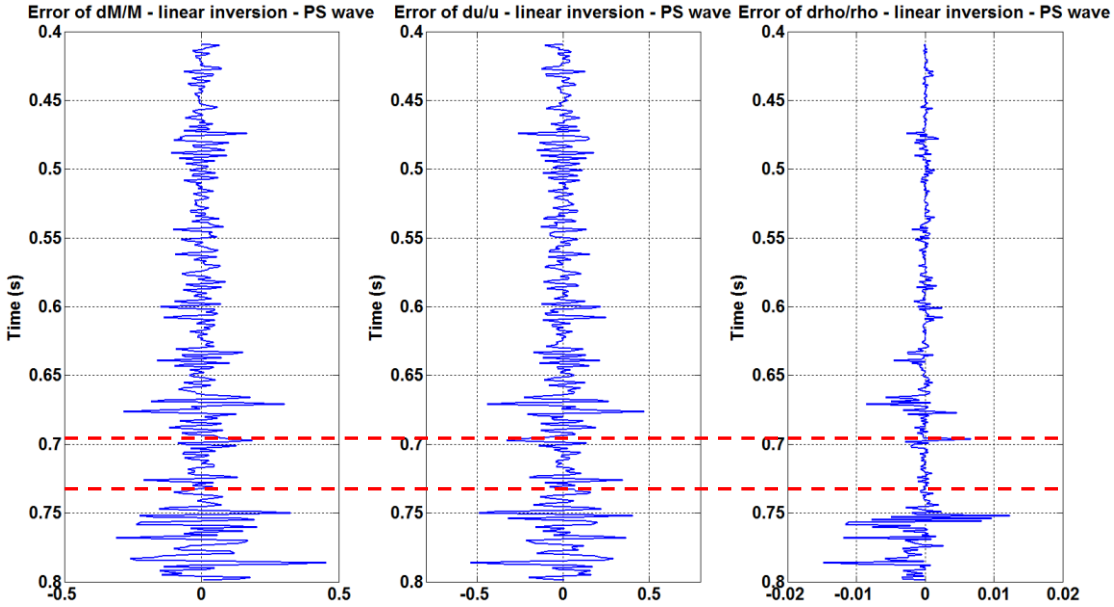

FIG. 23. Errors of inversed P-, S-wave modus, and density using linear inversion with PS-wave modelling data.

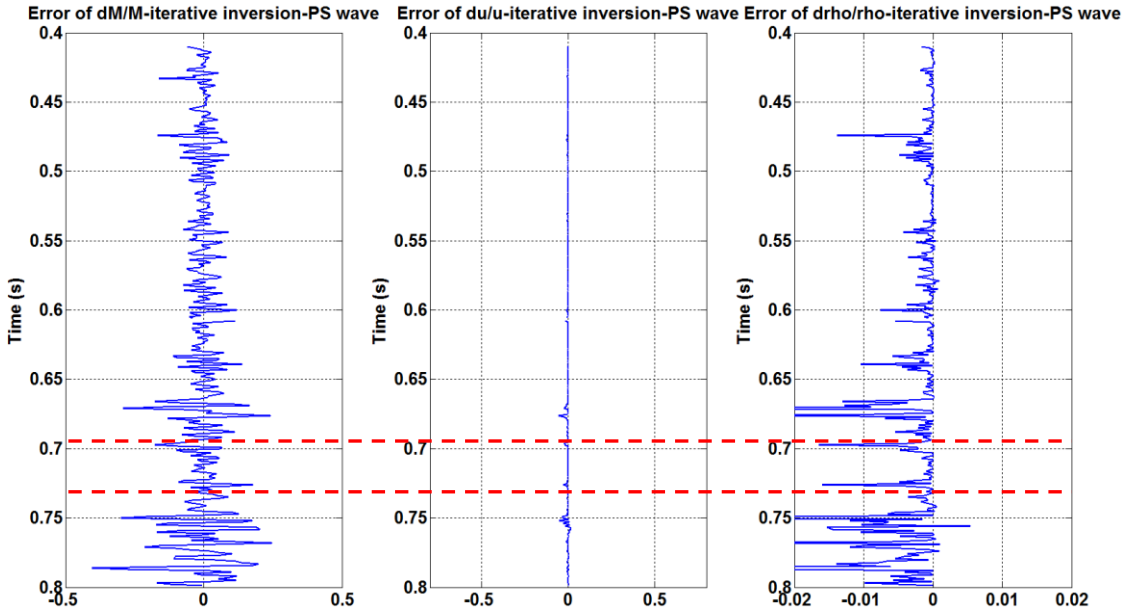

FIG. 24. Errors of inversed P-, S-wave modus, and density using non-linear AVO inversion with a combination of series reversion and Gauss-Newton with PS-wave modelling data.

Similarly, we calculated errors of estimated P-, S- wave modulus and density for both algorithms, which are shown in Figure 23 and 24 respectively. And the inversion of S-wave modulus using non-linear iterative method is much more acceptable than the linear inversed result.

CONCLUSION

In this paper, starting from Zoeppritz equation, we derived AVO/AVA series approximation in terms of P- and S- wave moduli for R_{pp} and R_{ps} in perturbation form and in ratio form. After that, the accuracy comparisons and the effect of high-order effect for R_{pp} and R_{ps} were discussed. The 2nd order truncated R_{pp} in ratio form with angle incidence was recommended to apply the non-linear AVO/AVA inversion with series reversion and Gauss-Newton method. To solve for the local convergence problem of Gauss-Newton iterative method, we solved the first order term of series reversion and considered it as the initial value for non-linear AVO/AVA with Gauss-Newton iterative algorithm. Eventually, AVO well synthetic angle gather both for PP- and PS- wave were applied into this new non-linear AVO/AVA method to examine the resolution of the AVO series approximated formula. According to comparisons and discussions, this new AVO/AVA approximation and the non-linear inversion method are advisable and efficient way to achieve a better answer.

ACKNOWLEDGEMENTS

This work was funded by CREWES industrial sponsors and NSERC (Natural Science and Engineering Research Council of Canada) through the grant CRDPJ 461179-13. The authors thank the sponsors of CREWES for continued support. We also thank Dr. Chen for his suggestion and discussion. All CREWES personnel researchers would be grateful acknowledged.

REFERENCE

Biot, M. a., 1941. General theory of three-dimensional consolidation. *Journal of Applied Physics*, 12(2), pp.155–164.

Gray, D., Goodway, B. & Chen, T., 1999. Bridging the Gap : Using AVO to detect changes in fundamental elastic constants. *SEG Technical Program Expanded Abstracts*.

K.~A.~Innanen, 2011. Inversion of the seismic AVF/AVA signatures of highly attenuative targets. *Geophysics*, 76, pp.1–14.

Krief, M. et al., 1990. A petrophysical interpretation using the velocities of P and S waves (full-waveform sonic). *The Log Analyst*, 31, pp.355–369.

Mavko, G., Mukerji, T. & Dvorkin, J., 1993. The rock physics handbook, 1998. *Cambridge University press*.

Russell, B.H. et al., 2003. Fluid-property discrimination with AVO: A Biot-Gassmann perspective. *Geophysics*, 68(1), pp.29–39.

Zoeppritz, K., 1919, Erdbebenwellen VIII B, Uber Reflexion and Durchgang Seismischer Wellen Duch Unstetigkeitsflachen: Gottinger Nachr., 1, 66-84.

Zong, Z., Yin, X. & Wu, G., 2012. AVO inversion and poroelasticity with P-and S-wave moduli. *Geophysics*, 77(6), pp.N17–N24.

APPENDIX I: R_{PP}, R_{PS} IN PERTURBATION FORM

The explicit weighting factors of R_{pp} and R_{ps} in perturbation forms are shown in this appendix.

$$R_{pp} = R_{pp}^{(1)} + R_{pp}^{(2)} + R_{pp}^{(3)} + \cdots; \tag{I.1}$$

$$R_{ps} = R_{ps}^{(1)} + R_{ps}^{(2)} + R_{ps}^{(3)} + \cdots; \tag{I.2}$$

I.1 First order poroelastic weighting factors of R_{PP} for a_M, a_μ, a_ρ

$$R_{pp}^{(1)} = \Gamma_M^{pp} a_M + \Gamma_\mu^{pp} a_\mu + \Gamma_\rho^{pp} a_\rho \tag{I.3}$$

$$\Gamma_M^{pp} = \frac{\sec^2\theta_0}{4} \tag{I.4}$$

$$\Gamma_\mu^{pp} = -\frac{2}{\gamma_{sat}^2}\sin^2\theta_0 \tag{I.5}$$

$$\Gamma_\rho^{pp} = \frac{1}{2} - \frac{\sec^2\theta_0}{4} \tag{I.6}$$

I.2 Second order poroelastic weighting factors of R_{PP} for a_M, a_μ, a_ρ

$$R_{pp}^{(2)} = \Gamma_{2M}^{pp} a_M^2 + \Gamma_{2\mu}^{pp} a_\mu^2 + \Gamma_{2\rho}^{pp} a_\rho^2 + \Gamma_{M\rho}^{pp} a_M a_\rho + \Gamma_{\mu\rho}^{pp} a_\mu a_\rho + \Gamma_{M\mu}^{pp} a_M a_\mu \tag{I.7}$$

$$\Gamma_{2M}^{pp} = \frac{1}{8}\left(1 + 2\sin^2\theta_0\right) \tag{I.8}$$

$$\Gamma_{2\mu}^{pp} = \frac{1}{\gamma_{sat}^2}\left(\frac{1}{\gamma_{sat}} - 2\right)\sin^2\theta_0 \tag{I.9}$$

$$\Gamma_{2\rho}^{pp} = \frac{1}{8}\left(1 - \frac{2}{\gamma_{sat}}\sin^2\theta_0\right) \tag{I.10}$$

$$\Gamma_{M\rho}^{pp} = -\frac{1}{4}\sin^2\theta_0 \tag{I.11}$$

$$\Gamma_{\mu\rho}^{pp} = \frac{\sin^2\theta_0}{\gamma_{sat}^2} \tag{I.12}$$

$$\Gamma_{M\mu}^{pp} = 0 \tag{I.13}$$

I.3 Third order poroelastic weighting factors of R_{PP} for a_M, a_μ, a_ρ

$$\begin{aligned} R_{pp}^{(3)} = {} & \Gamma_{3M}^{pp} a_M^3 + \Gamma_{3\mu}^{pp} a_\mu^3 + \Gamma_{3\rho}^{pp} a_\rho^3 + \Gamma_{2\mu\rho}^{pp} a_\mu^2 a_\rho + \Gamma_{2\mu M}^{pp} a_\mu^2 a_M + \Gamma_{\mu 2\rho}^{pp} a_\mu a_\rho^2 \\ & + \Gamma_{\mu 2M}^{pp} a_\mu a_M^2 + \Gamma_{M2\rho}^{pp} a_M a_\rho^2 + \Gamma_{\rho 2M}^{pp} a_\rho a_M^2 + \Gamma_{M\mu\rho}^{pp} a_M a_\mu a_\rho \end{aligned} \tag{I.14}$$

$$\Gamma_{3M}^{pp} = \frac{1}{64}\left(5+15\sin^2\theta_0\right) \tag{I.15}$$

$$\Gamma_{3\mu}^{pp} = \frac{1}{4}\frac{1}{\gamma_{sat}^2}\left(\frac{7}{\gamma_{sat}}-8\right)\sin^2\theta_0 \tag{I.16}$$

$$\Gamma_{3\rho}^{pp} = \frac{5}{64}+\left(\frac{1}{64}-\frac{3}{16}\frac{1}{\gamma_{sat}}\right)\sin^2\theta_0 \tag{I.17}$$

$$\Gamma_{2\mu\rho}^{pp} = -\frac{1}{4\gamma_{sat}^2}\left(\frac{3}{\gamma_{sat}}-5\right)\sin^2\theta_0 \tag{I.18}$$

$$\Gamma_{2\mu M}^{pp} = -\frac{1}{2}\frac{1}{\gamma_{sat}^3}\sin^2\theta_0 \tag{I.19}$$

$$\Gamma_{\mu 2\rho}^{pp} = \frac{1}{16\gamma_{sat}}(\frac{6}{\gamma_{sat}}-1)\sin^2\theta_0 \tag{I.20}$$

$$\Gamma_{\mu 2M}^{pp} = \frac{1}{8\gamma_{sat}^2}\sin^2\theta_0 \tag{I.21}$$

$$\Gamma_{M2\rho}^{pp} = -\frac{1}{64}+\left(-\frac{1}{8\gamma_{sat}}+\frac{1}{64}\right)\sin^2\theta_0 \tag{I.22}$$

$$\Gamma_{\rho 2M}^{pp} = -\frac{1}{64}-\frac{17}{64}\sin^2\theta_0 \tag{I.23}$$

$$\Gamma_{M\mu\rho}^{pp} = \frac{1}{4\gamma_{sat}^2}\sin^2\theta_0 \tag{I.24}$$

I.4 First order poroelastic weighting factors of R_{PS} for a_M , a_μ , a_ρ

$$R_{ps}^{(1)} = \Gamma_M^{ps}a_M + \Gamma_\mu^{ps}a_\mu + \Gamma_\rho^{ps}a_\rho \tag{I.25}$$

$$\Gamma_M^{ps} = 0 \tag{I.26}$$

$$\Gamma_\mu^{ps} = -\frac{1}{\gamma_{sat}}\sin\theta_0 \tag{I.27}$$

$$\Gamma_\rho^{ps} = -\frac{1}{2}\sin\theta_0 \tag{I.28}$$

I.5 Second order poroelastic weighting factors of R_{PS} for a_M , a_μ , a_ρ

$$R_{ps}^{(2)} = \Gamma_{2M}^{ps}a_M^2 + \Gamma_{2\mu}^{ps}a_\mu^2 + \Gamma_{2\rho}^{ps}a_\rho^2 + \Gamma_{M\rho}^{ps}a_M a_\rho + \Gamma_{\mu\rho}^{ps}a_\mu a_\rho + \Gamma_{M\mu}^{ps}a_M a_\mu \tag{I.29}$$

$$\Gamma_{2M}^{ps} = 0 \tag{I.30}$$

$$\Gamma_{2\mu}^{ps} = -\frac{3}{4}\frac{1}{\gamma_{sat}}\sin\theta_0 \tag{I.31}$$

$$\Gamma_{2\rho}^{ps} = -\frac{1}{4}\sin\theta_0 \tag{I.32}$$

$$\Gamma_{M\rho}^{ps} = -\frac{1}{8}\sin\theta_0 \tag{I.33}$$

$$\Gamma_{\mu\rho}^{ps} = \left(-\frac{1}{8}+\frac{1}{2\gamma_{sat}}\right)\sin\theta_0 \tag{I.34}$$

$$\Gamma_{M\mu}^{ps} = \frac{1}{4\gamma_{sat}}\sin\theta_0 \tag{I.35}$$

I.6 Third order poroelastic weighting factors of $\mathbf{R_{PS}}$ for a_M , a_μ , a_ρ

$$\begin{aligned} R_{ps}^{(3)} = {} & \Gamma_{3M}^{ps}a_M^3 + \Gamma_{3\mu}^{ps}a_\mu^3 + \Gamma_{3\rho}^{ps}a_\rho^3 + \Gamma_{2\mu\rho}^{ps}a_\mu^2 a_\rho + \Gamma_{2\mu M}^{ps}a_\mu^2 a_M + \Gamma_{\mu 2\rho}^{ps}a_\mu a_\rho^2 \\ & + \Gamma_{\mu 2M}^{ps}a_\mu a_M^2 + \Gamma_{M2\rho}^{ps}a_M a_\rho^2 + \Gamma_{\rho 2M}^{ps}a_\rho a_M^2 + \Gamma_{M\mu\rho}^{ps}a_M a_\mu a_\rho \end{aligned} \tag{I.36}$$

$$\Gamma_{3M}^{ps} = 0 \tag{I.37}$$

$$\Gamma_{3\mu}^{ps} = -\frac{5}{8}\frac{1}{\gamma_{sat}}\sin\theta_0 \tag{I.38}$$

$$\Gamma_{3\rho}^{ps} = -\frac{5}{32}\sin\theta_0 \tag{I.39}$$

$$\Gamma_{2\mu\rho}^{ps} = \left(-\frac{1}{16}+\frac{7}{16\gamma_{sat}}\right)\sin\theta_0 \tag{I.40}$$

$$\Gamma_{2\mu M}^{ps} = \frac{3}{16}\frac{1}{\gamma_{sat}}\sin\theta_0 \tag{I.41}$$

$$\Gamma_{\mu 2\rho}^{ps} = \left(-\frac{1}{32}+\frac{3}{16}\frac{1}{\gamma_{sat}}\right)\sin\theta_0 \tag{I.42}$$

$$\Gamma_{\mu 2M}^{ps} = \frac{1}{8}\frac{1}{\gamma_{sat}}\sin\theta_0 \tag{I.43}$$

$$\Gamma_{M2\rho}^{ps} = -\frac{1}{32}\sin\theta_0 \tag{I.44}$$

$$\Gamma_{\rho 2M}^{ps} = -\frac{1}{16}\sin\theta_0 \tag{I.45}$$

$$\Gamma_{M\mu\rho}^{pp} = \left(-\frac{1}{32}-\frac{1}{16\gamma_{sat}}\right)\sin\theta_0 \tag{I.46}$$

APPENDIX II: R_{PP}, R_{PS} IN RATIO FORM

The explicit weighting factors of R_{pp} and R_{ps} in ratio forms are shown in this appendix.

$$R_{pp} = R_{pp}^{(1)} + R_{pp}^{(2)} + R_{pp}^{(3)} + \cdots; \tag{II.1}$$

$$R_{ps} = R_{ps}^{(1)} + R_{ps}^{(2)} + R_{ps}^{(3)} + \cdots; \tag{II.2}$$

II.1 First order poroelastic weighting factors of R_{PP} for $\Delta M/M$, $\Delta\mu/\mu$, $\Delta\rho/\rho$

$$R_{pp}^{(1)} = \Lambda_M^{pp}\frac{\Delta M}{M} + \Lambda_\mu^{pp}\frac{\Delta\mu}{\mu} + \Lambda_\rho^{pp}\frac{\Delta\rho}{\rho} \tag{II.3}$$

$$\Lambda_M^{pp} = \frac{\sec^2\theta_0}{4} \tag{II.4}$$

$$\Lambda_\mu^{pp} = -\frac{2}{\gamma_{sat}^2}\sin^2\theta_0 \tag{II.5}$$

$$\Lambda_\rho^{pp} = \frac{1}{2} - \frac{\sec^2\theta_0}{4} \tag{II.6}$$

II.2 Second order poroelastic weighting factors of R_{PP} for $\Delta M/M$, $\Delta\mu/\mu$, $\Delta\rho/\rho$

$$\begin{aligned} R_{pp}^{(2)} = {} & \Lambda_{2M}^{pp}\left(\frac{\Delta M}{M}\right)^2 + \Lambda_{2\mu}^{pp}\left(\frac{\Delta\mu}{\mu}\right)^2 + \Lambda_{2\rho}^{pp}\left(\frac{\Delta\rho}{\rho}\right)^2 + \Lambda_{M\mu}^{pp}\frac{\Delta M}{M}\frac{\Delta\mu}{\mu} \\ & + \Lambda_{M\rho}^{pp}\frac{\Delta M}{M}\frac{\Delta\rho}{\rho} + \Lambda_{\mu\rho}^{pp}\frac{\Delta\mu}{\mu}\frac{\Delta\rho}{\rho} \end{aligned} \tag{II.7}$$

$$\Lambda_{2M}^{pp} = \frac{1}{8}\sin^2\theta_0 \tag{II.8}$$

$$\Lambda_{2\mu}^{pp} = \frac{1}{\gamma_{sat}^2}\left(\frac{1}{\gamma_{sat}} - 1\right)\sin^2\theta_0 \tag{II.9}$$

$$\Lambda_{2\rho}^{pp} = \left(-\frac{2}{4\gamma_{sat}} + \frac{1}{8}\right)\sin^2\theta_0 \tag{II.10}$$

$$\Lambda_{M\rho}^{pp} = -\frac{1}{4}\sin^2\theta_0 \tag{II.11}$$

$$\Lambda_{\mu\rho}^{pp} = \frac{1}{\gamma_{sat}^2}\sin^2\theta_0 \tag{II.12}$$

$$\Gamma_{M\mu}^{pp} = 0 \tag{II.13}$$

II.3 Third order poroelastic weighting factors of R_{PP} for $\Delta M/M$, $\Delta\mu/\mu$, $\Delta\rho/\rho$

$$R_{pp}^{(3)} = \Lambda_{3M}^{pp}\left(\frac{\Delta M}{M}\right)^3 + \Lambda_{3\mu}^{pp}\left(\frac{\Delta\mu}{\mu}\right)^3 + \Lambda_{3\rho}^{pp}\left(\frac{\Delta\rho}{\rho}\right)^3 + \Lambda_{2\mu\rho}^{pp}\left(\frac{\Delta\mu}{\mu}\right)^2\frac{\Delta\rho}{\rho} + \Lambda_{2\mu M}^{pp}\left(\frac{\Delta\mu}{\mu}\right)^2\frac{\Delta M}{M} + \Lambda_{\mu 2\rho}^{pp}\frac{\Delta\mu}{\mu}\left(\frac{\Delta\rho}{\rho}\right)^2 + \Lambda_{\mu 2M}^{pp}\frac{\Delta\mu}{\mu}\left(\frac{\Delta M}{M}\right)^2 + \Lambda_{M2\rho}^{pp}\frac{\Delta M}{M}\left(\frac{\Delta\rho}{\rho}\right)^2 + \Lambda_{\rho 2M}^{pp}\frac{\Delta\rho}{\rho}\left(\frac{\Delta M}{M}\right)^2 + \Lambda_{M\mu\rho}^{pp}\frac{\Delta M}{M}\frac{\Delta\mu}{\mu}\frac{\Delta\rho}{\rho} \quad \text{(II.14)}$$

$$\Lambda_{3M}^{pp} = \frac{1}{64}\left(1+3\sin^2\theta_0\right) \quad \text{(II.15)}$$

$$\Lambda_{3\mu}^{pp} = \frac{1}{4}\frac{1}{\gamma_{sat}^2}\left(\frac{3}{\gamma_{sat}}-2\right)\sin^2\theta_0 \quad \text{(II.16)}$$

$$\Lambda_{3\rho}^{pp} = \frac{1}{64}+\left(-\frac{3}{64}+\frac{1}{16\gamma_{sat}}\right)\sin^2\theta_0 \quad \text{(II.17)}$$

$$\Lambda_{2\mu\rho}^{pp} = -\frac{3}{4}\frac{1}{\gamma_{sat}^2}\left(\frac{1}{\gamma_{sat}}-1\right)\sin^2\theta_0 \quad \text{(II.18)}$$

$$\Lambda_{2\mu M}^{pp} = -\frac{1}{2}\frac{1}{\gamma_{sat}^3}\sin^2\theta_0 \quad \text{(II.19)}$$

$$\Lambda_{\mu 2\rho}^{pp} = -\frac{1}{16\gamma_{sat}}\left(\frac{2}{\gamma_{sat}}+1\right)\sin^2\theta_0 \quad \text{(II.20)}$$

$$\Lambda_{\mu 2M}^{pp} = \frac{1}{8\gamma_{sat}^2}\sin^2\theta_0 \quad \text{(II.21)}$$

$$\Lambda_{M2\rho}^{pp} = -\frac{1}{64}+\left(-\frac{1}{8\gamma_{sat}}+\frac{9}{64}\right)\sin^2\theta_0 \quad \text{(II.22)}$$

$$\Lambda_{\rho 2M}^{pp} = -\frac{1}{64}-\frac{9}{64}\sin^2\theta_0 \quad \text{(II.23)}$$

$$\Lambda_{M\mu\rho}^{pp} = \frac{1}{4\gamma_{sat}^2}\sin^2\theta_0 \quad \text{(II.24)}$$

II.4 First order poroelastic weighting factors of R_{PS} for $\Delta M/M$, $\Delta\mu/\mu$, $\Delta\rho/\rho$

$$R_{ps}^{(1)} = \Lambda_M^{ps}\frac{\Delta M}{M} + \Lambda_\mu^{ps}\frac{\Delta\mu}{\mu} + \Lambda_\rho^{ps}\frac{\Delta\rho}{\rho} \quad \text{(II.25)}$$

$$\Lambda_M^{ps} = 0 \quad \text{(II.26)}$$

$$\Lambda_{\mu}^{ps} = -\frac{1}{\gamma_{sat}}\sin\theta_0 \tag{II.27}$$

$$\Lambda_{\rho}^{ps} = -\frac{1}{2}\sin\theta_0 \tag{II.28}$$

II.5 Second order poroelastic weighting factors of R_{PS} for $\Delta M/M$, $\Delta\mu/\mu$, $\Delta\rho/\rho$

$$\begin{aligned} R_{ps}^{(2)} = {} & \Lambda_{2M}^{ps}\left(\frac{\Delta M}{M}\right)^2 + \Lambda_{2\mu}^{ps}\left(\frac{\Delta\mu}{\mu}\right)^2 + \Lambda_{2\rho}^{ps}\left(\frac{\Delta\rho}{\rho}\right)^2 + \Lambda_{M\mu}^{ps}\frac{\Delta M}{M}\frac{\Delta\mu}{\mu} \\ & + \Lambda_{M\rho}^{ps}\frac{\Delta M}{M}\frac{\Delta\rho}{\rho} + \Lambda_{\mu\rho}^{ps}\frac{\Delta\mu}{\mu}\frac{\Delta\rho}{\rho} \end{aligned} \tag{II.29}$$

$$\Lambda_{2M}^{ps} = 0 \tag{II.30}$$

$$\Lambda_{2\mu}^{ps} = -\frac{1}{4\gamma_{sat}}\sin\theta_0 \tag{II.31}$$

$$\Lambda_{2\rho}^{ps} = \frac{1}{8}\left(\frac{1}{\gamma_{sat}^2}+1\right)\sin^3\theta_0 \tag{II.32}$$

$$\Lambda_{M\rho}^{ps} = -\frac{1}{8}\sin\theta_0 \tag{II.33}$$

$$\Lambda_{\mu\rho}^{ps} = \left(-\frac{1}{8}+\frac{1}{2\gamma_{sat}}\right)\sin\theta_0 \tag{II.34}$$

$$\Lambda_{M\mu}^{ps} = \frac{1}{4\gamma_{sat}}\sin\theta_0 \tag{II.35}$$

II.6 Third order poroelastic weighting factors of R_{PS} for $\Delta M/M$, $\Delta\mu/\mu$, $\Delta\rho/\rho$

$$\begin{aligned} R_{ps}^{(3)} = {} & \Lambda_{3M}^{ps}\left(\frac{\Delta M}{M}\right)^3 + \Lambda_{3\mu}^{ps}\left(\frac{\Delta\mu}{\mu}\right)^3 + \Lambda_{3\rho}^{ps}\left(\frac{\Delta\rho}{\rho}\right)^3 + \Lambda_{2\mu\rho}^{ps}\left(\frac{\Delta\mu}{\mu}\right)^2\frac{\Delta\rho}{\rho} \\ & + \Lambda_{2\mu M}^{ps}\left(\frac{\Delta\mu}{\mu}\right)^2\frac{\Delta M}{M} + \Lambda_{\mu 2\rho}^{ps}\frac{\Delta\mu}{\mu}\left(\frac{\Delta\rho}{\rho}\right)^2 + \Lambda_{\mu 2M}^{ps}\frac{\Delta\mu}{\mu}\left(\frac{\Delta M}{M}\right)^2 \\ & + \Lambda_{M2\rho}^{ps}\frac{\Delta M}{M}\left(\frac{\Delta\rho}{\rho}\right)^2 + \Lambda_{M\mu\rho}^{ps}\frac{\Delta M}{M}\frac{\Delta\mu}{\mu}\frac{\Delta\rho}{\rho} \end{aligned} \tag{II.36}$$

$$\Lambda_{3M}^{ps} = 0 \tag{II.37}$$

$$\Lambda_{3\mu}^{ps} = -\frac{1}{8}\frac{1}{\gamma_{sat}}\sin\theta_0 \tag{II.38}$$

$$\Lambda_{3\rho}^{ps} = -\frac{1}{32}\sin\theta_0 \tag{II.39}$$

$$\Lambda_{2\mu\rho}^{ps} = \frac{3}{16}\frac{1}{\gamma_{sat}}\sin\theta_0 \tag{II.40}$$

$$\Lambda_{2\mu M}^{ps} = \frac{1}{16\gamma_{sat}}\sin\theta_0 \tag{II.41}$$

$$\Lambda_{\mu 2\rho}^{ps} = \left(\frac{1}{32} - \frac{1}{16}\frac{1}{\gamma_{sat}}\right)\sin\theta_0 \tag{II.42}$$

$$\Lambda_{\mu 2M}^{ps} = \frac{1}{8}\frac{1}{\gamma_{sat}}\sin^3\theta_0 \tag{II.43}$$

$$\Lambda_{M2\rho}^{ps} = \frac{1}{32}\sin\theta_0 \tag{II.44}$$

$$\Lambda_{\rho 2M}^{ps} = -\frac{1}{16}\sin^3\theta_0 \tag{II.45}$$

$$\Lambda_{M\mu\rho}^{pp} = \left(-\frac{1}{32} - \frac{1}{16\gamma_{sat}}\right)\sin\theta_0 \tag{II.46}$$